Enclosure 2

Metallic Materials Qualification for the Kairos Power Fluoride Salt-Cooled High-Temperature Reactor, Revision 4

(Non-Proprietary)

KP-TR-013-NP

Kairos Power LLC
707 W. Tower Ave
Alameda, CA 94501

Metallic Materials Qualification for the Kairos Power Fluoride Salt-Cooled High-Temperature Reactor

Topical Report

Revision No. 4
Document Date: September 2022

Non-Proprietary

COPYRIGHT Notice

Rev	Description of Change	Date
0	Initial Issuance	June 2020
1	Addition of Non-Power Test Reactor information and response to NRC questions dated November 25, 2020	June 2021
2	Response to NRC questions dated October 13, 2021 and elimination of the PHRS for the Non-Power Test Reactor	April 2022
3	Revise wording on contaminant testing with intermediate coolant; Revise SSRT testing temperatures and add 750°C creep test and change test to Nominal Flibe; Incorporate editorial corrections	August 2022
4	Revise *R*-ratio for fatigue testing from 0.9 to 0.1. Revise fatigue crack growth rate and added Figure 33.	September 2022

EXECUTIVE SUMMARY

This Topical Report describes the qualification plans for structural alloys used in the safety-related systems of reactors utilizing Kairos Power Fluoride Salt-Cooled High Temperature Reactor (KP-FHR) technology. The plans described herein are applicable to KP-FHR power and non-power (test) reactors. These reactors operate near atmospheric pressure, utilize high temperature fuel and use molten salt coolants to provide a high degree of passive safety.

This document describes the testing and modelling required to qualify the structural alloys used in the safety-related portion of the plants, i.e., the fluoride salt-cooled reactor system. In the reactor system, the reactor vessel is the primary safety-related component, as it serves to maintain Flibe coolant around the fuel in the reactor core. This report does not describe nor does it apply to material qualification for non-safety-related systems or components. Specifically, this report describes work to extend the ASME qualification of structural alloys to higher temperatures, to generate data in high temperature air that facilitates design, and to demonstrate environmental compatibility of the structural materials. The environmental compatibility testing for the commercial power reactor and a limited scope test plan for the shorter-lived non-power test reactor are detailed in the body of the report. Additionally, this report presents, for information, ongoing work to develop coatings and cladding and reliability and integrity management plans.

Kairos Power is requesting Nuclear Regulatory Commission review and approval of the qualification plan described in this report for metallic structural materials used in Flibe-wetted areas for safety-significant high temperature components of the reactors for use by licensing applicants under 10 CFR 50 or 10 CFR 52. This includes approval of the planned testing and analyses to address the materials reliability and environmental compatibility issues via design, operation, and inspection. The results of these planned tests and analyses, along with a description of the design and inspection program will be provided in a future license application.

Table of Contents

LIST OF ABBREVIATIONS

Acronym	Definition
ASME	American Society for Mechanical Engineers
ASTM	American Society for Testing and Materials
BWR	Boiling Water Reactor
CFR	Code of Federal Regulations
DPA	Displacements per Atom
DOE	Department of Energy
EAC	Environmentally Assisted Cracking
FHR	Fluoride Salt-Cooled High Temperature Reactor
FSAR	Final Safety Analysis Report
HFIR	High Flux Isotope Reactor
IASCC	Irradiation-Assisted Stress Corrosion Cracking
IGSCC	Intergranular Stress Corrosion Cracking
KP-FHR	Kairos Power Fluoride Salt-Cooled High Temperature Reactor
LWA	Limited Work Authorization
LWR	Light Water Reactors
MANDE	Monitoring and Non-Destructive Examination
MHTGR	Modular High Temperature Gas Reactor
MSR	Molten Salt Reactor
MSRE	Molten Salt Reactor Experiment
NRC	Nuclear Regulatory Commission
OFHC	Oxygen-Free, High-Conductivity
ORNL	Oak Ridge National Laboratory
PDC	Principal Design Criteria
PIRT	Phenomena Identification and Ranking Table
PSAR	Preliminary Safety Analysis Report
PWR	Pressurized Water Reactor
RCL	Rotating Cage Loop
RG	Regulatory Guide
RIM	Reliability and Integrity Management
SCC	Stress Corrosion Cracking
SFR	Sodium-Cooled Fast Reactor
SSC	Structure, System, or Component
SSRT	Slow Strain Rate Testing
TRISO	Tri-Structural Isotropic

1 INTRODUCTION (INFORMATION)

Kairos Power LLC (Kairos Power) is pursuing the design, licensing, and deployment of reactors based on Fluoride Salt-Cooled High Temperature Reactor (KP-FHR) technology. Material qualification programs designed for both a non-power test reactor (Hermes) and a commercial power reactor (KP-X) are being conducted to support these objectives. To construct these reactors, Kairos Power will rely on the use of structural alloys that are qualified for use at high temperatures in selected applications. The materials qualification program relies on materials testing, materials modeling, and inspection and monitoring programs to ensure the performance of the safety-related reactor systems. This report details the approach for safety-related metallic structural materials qualification in Flibe-wetted areas for the KP-FHR consistent with American Society of Mechanical Engineers (ASME) Section III Division 5 (Rules for Construction of Nuclear Power Plant Components, High Temperature Reactors) requirements. The non-power test reactor application is implementing a quality assurance program based on ANSI/ANS-15.8-1995, "Quality Assurance Program Requirements for Research Reactors," (ANSI/ANS-15.8), which is endorsed by NRC Regulatory Guide 2.5, "Quality Assurance Program Requirements for Research and Test Reactors." For this reason, Kairos Power is departing from the Division 5 code requirements that would require an NQA-1 based quality assurance program for the non-power test reactor. Based on the Phenomena Identification and Ranking Table (PIRT) conducted for the commercial power reactor, this report defines a subset of work required for the non-power test reactor as well as the full set of tests for the commercial power reactor. At the completion of each of these testing programs, appropriate environmental degradation factors for the non-power test reactor and commercial power reactor can be set and satisfy ASME Section III Division 5 requirements.

The structural alloys for use in the safety-related Flibe-wetted areas of the reactor were selected considering their properties, commercial availability and if the material is qualified for use via ASME Section III Division 5. These rules for construction require demonstration of the environmental compatibility of the structural materials. A PIRT-type process as described in Regulatory Guide (RG) 1.203, "Transient and Accident Analysis Methods" (Reference 1) was used to identify significant degradation phenomena and to develop the testing and modelling qualification presented in this report. Based on the PIRT conducted, a subset of work required for the non-power test reactor as well as the full set of tests required for the commercial power reactor are provided herein.

The design of the safety-related Flibe-wetted areas of the reactor does not require the application of cladding or coatings [[

]] . If coatings or cladding are used in the safety-related Flibe-wetted portions of the reactor, their use in the design will be in a manner consistent with ASME Code rules. For example, ASME Section III, Division 5, Subsection HB, Subpart B for structural load carrying Class A materials (Reference 2).

This report also presents an overview of an Inspection and Monitoring program (non-power test reactor and commercial power reactor) and a Reliability & Integrity Management (RIM) program (commercial power reactor) for information. The Inspection and Monitoring program further ensures material and component performance will be attained. These efforts will involve on-line monitoring systems as well as periodic inspections. The Inspection and Monitoring program for the non-power test reactor will be described as part of the operating license application. The RIM program is an integral part of nuclear component life cycle management. The unique physical features of high temperature reactors such as the

KP-FHR presents a new paradigm for RIM that has required the Code to develop new approaches. The new approach being implemented as ASME Section XI, Division 2, "Reliability", applies to any type of reactor design and was published for the first time in the 2019 Edition. A RIM program will be described as part of the operating licensing application for a commercial power reactor.

1.1 DESIGN OF THE KP-FHR

To facilitate NRC review and approval of this report, design features considered essential to the KP-FHR technology are provided in this section. These key features are not expected to change during the ongoing detailed design work by Kairos Power and provide the basis to support the safety review. Should fundamental changes occur to these design features or revised regulations be promulgated that affect the conclusions in this report, such changes will be reconciled and addressed in future license application submittals.

1.1.1 Design Overview

The KP-FHR is a U.S.-developed Generation IV advanced reactor technology. In the last decade, U.S. National Laboratories and Universities have developed conceptual Fluoride Salt-Cooled High Temperature Reactor (FHR) designs with different fuel geometries, core configurations, heat transport systems, power cycles, and power levels. More recently, the University of California at Berkeley developed the Mark 1 pebble-bed FHR, incorporating lessons learned from the previous decade of designs (Reference 3). Kairos Power has built on the foundation laid by Department of Energy (DOE)-sponsored, University-led Integrated Research Projects to develop the KP-FHR for both a non-power test reactor (Hermes) and a commercial power reactor (KP-X). Although not intended to support the findings necessary to approve this report, additional design description information is provided in the "Design Overview of the Kairos Power Fluoride Salt-Cooled High Temperature Reactor" Technical Report (Reference 4).

1.1.2 Design Background

Kairos Power is developing both a non-power test reactor and a commercial power generation reactor based on KP-FHR technology. The operating parameters discussed in this topical report will apply to both reactor classes. The non-power test reactor will operate at lower power level and potentially lower temperatures than the power reactor. For the purposes of the metallic material qualification, the operating parameters for the power reactor are considered to bound those that will exist in the test reactor. One difference that will have a bearing on data needed to qualify the metallic material is the expected lifetime of the safety-related Flibe-wetted components in the reactor. The non-power reactor component lifetime is expected to be limited to 5 years, while the component lifetime in the power reactor will be [[ ]]. The key features of the power and non-power reactors are compared in Table 1.

1.1.3 Key Features

The KP-FHR technology integrates key design features and material choices into a physically compact, intrinsically safe, high temperature reactor which will be built with existing, industrially proven materials. Key design features of the KP-FHR include the use of high temperature fuel, high boiling point molten salt coolants, and low-pressure operation. This combination of the Tri-Structural Isotropic (TRISO) particle fuel, stable high boiling temperature fluoride salt coolant, and low operating stresses results in a robust

reactor design with intrinsic passive safety. Notably, the reactor vessel is expected to see relatively low levels of irradiation damage, <0.1 dpa for the lifetime of both the non-power and power reactors.

The fuel in the KP-FHR is based on the TRISO high temperature fuel. TRISO fuel is a carbon matrix coated particle fuel, originally developed for high temperature gas-cooled reactors, in a pebble-shaped fuel element. Coatings on the particle fuel provide retention of fission products to temperatures approaching 1600°C. The primary coolant that is used in safety-related systems is a mixture of lithium fluoride (LiF) and beryllium fluoride (BeF_2) salts in a ratio of approximately 2:1. This F-Li-Be based salt, i.e., 'Flibe' has been proven as an effective nuclear coolant in the Molten Salt Reactor Experiment (MSRE) research program and the operation of the MSRE nuclear reactor (Reference 74). Furthermore, there has been significant research into the stability and compatibility of Flibe in nuclear applications since the operation of the MSRE. The KP-FHR is a low-pressure reactor which operates with a modest overpressure (~0.2 MPa or 2 atm) in the reactor vessel head space to minimize contamination of the primary coolant. The low-pressure operation and associated low operating stresses are another key design feature of the KP-FHR. Low operating stresses help enable the use of conventional structural alloys and provides significant margin against high temperature failure modes such as creep-rupture.

1.1.3.1 Heat Transport Systems

The commercial power reactor is expected to include at least two heat transfer loops. A primary loop contains Flibe and maintains cooling in the core. Another heat transfer loop(s) removes heat from the primary system during normal operations. Figure 2 shows two heat transport loops for the power reactor and the operating temperature range (550-650°C). The non-power test reactor will include the primary loop and provide a heat rejection subsystem which will include a heat rejection radiator, heat rejection blower and associated ducting. For both the non-power and power reactor, the hot leg of the primary heat transport loop is anticipated to operate up to 650°C and the cold leg returns the Flibe to the reactor vessel at 550°C.

The KP-FHR design includes two decay heat removal systems. A system for providing decay heat removal is used following normal shutdowns and a separate passive decay heat removal system, [[ ]] removes decay heat in response to postulated events. Note that the passive decay heat removal system does not rely on electrical power to accomplish its safety function.

1.1.3.2 Containment Approach

The KP-FHR design uses a functional containment approach, like the Modular High Temperature Gas-Cooled Reactor (MHTGR) rather than a low-leakage, pressure-retaining containment structure that is typically used for light water reactors (LWRs). The KP-FHR functional containment safety design objective is to meet 10 CFR 50.34 (10 CFR 52.79) offsite dose requirements at the plant's exclusion area boundary with margin. A functional containment is defined in RG 1.232, "Guidance for Developing Principal Design Criteria for Non-Light Water Reactors" as a "barrier, or set of barriers taken together, that effectively limit the physical transport and release of radionuclides to the environment across a full range of normal operating conditions, anticipated operational occurrences, and accident conditions. RG 1.232 includes an example design criterion for the functional containment (MHTGR Criterion 16). As also stated in RG 1.232, the NRC has reviewed the functional containment concept and found it "generally acceptable," provided

that “appropriate performance requirements and criteria” are developed. The NRC staff has developed a proposed methodology for establishing functional containment performance criteria for non-LWRs, which is presented in SECY-18-0096, “Functional Containment Performance Criteria for Non-Light-Water-Reactors”. This SECY document has been approved by the Commission.

The functional containment approach for the KP-FHR is to control radionuclides primarily at their source within the coated fuel particle under normal operations and accident conditions without requiring active design features or operator actions. The KP-FHR design relies primarily on the multiple barriers within the TRISO fuel particles and fuel pebble to ensure that the dose at the site boundary (from postulated accidents) meets regulatory limits. Additionally, in the KP-FHR (but not in MHTGR designs), the molten salt coolant serves as an additional barrier providing retention of fission products that could escape the fuel particle and fuel pebble barriers. This additional retention barrier is a key feature of the enhanced safety and reduced source term in the KP-FHR. To enable fission product retention of the Flibe coolant, the reactor vessel must retain the coolant around the fuel pebbles. Thus, the reactor vessel is considered to be a safety-related structure. [[

]]

1.1.3.3 Reactor Vessel

The anticipated design of the KP-FHR reactor vessel is based on a vertical cylinder with bottom and top heads. The vessel is expected to be constructed from materials that are qualified by the ASME Section III. The reactor vessel serves as part of the reactor coolant boundary and supports and interfaces with other systems such as rod control, pebble handling, and heat removal systems. The reactor vessel will be designed to withstand the operational loads imparted on it by the core structures, fuel, and coolant. Additionally, the reactor vessel will be of sufficient strength and resiliency to withstand off-nominal conditions required by ASME Section III Division 5 Level B, C, and D Service Conditions (Reference 37).

[[

]]

1.2 REGULATORY INFORMATION

1.2.1 Regulations Relevant to the KP-FHR Material Qualification

The KP-FHR is anticipated to be licensed under Title 10 of the Code of Federal Regulations (10 CFR) using a licensing pathway provided in Part 50 or Part 52. Applicants for construction permits for facilities licensed under 10 CFR 50 are required to provide a Preliminary Safety Analysis Report (PSAR), which provides a safety assessment of the facility in accordance with 10 CFR 50.34(a). Applicants for a Limited Work authorization (LWA) are required to submit a safety analysis that meets 10 CFR 50.34 for the scope of the LWA per 10 CFR 50.10(d)(3)(i). Subsections within 10 CFR 50.34(a) relevant to the requirement to describe design characteristics of the KP-FHR high temperature materials are listed below (note these are required to be updated as part of the operating license application in the Final Safety Evaluation Report (FSAR) per 10 CFR 50.34(b)(4)):

50.34(a)(1)(ii)(B) The extent to which generally accepted engineering standards are applied to the design of the reactor.

50.34(a)(1)(ii)(C) The extent to which the reactor incorporates unique, unusual or enhanced safety features having a significant bearing on the probability or consequences of accidental release of radioactive materials.

50.34(a)(2) A summary description and discussion of the facility, with special attention to design and operating characteristics, unusual or novel design features, and principal safety considerations.

50.34(a)(3)(ii) The preliminary design of the facility including the design bases and the relation of the design bases to the principal design criteria.

Similarly, applicants for combined licenses for facilities licensed under 10 CFR 52 are required to provide a FSAR which provides a safety assessment of the facility in accordance with 10 CFR 52.79. Subsections relevant to the design and performance of high temperature materials are as follows:

52.79(a)(2) A description and analysis of the structures, systems, and components of the facility with emphasis upon performance requirements, the bases, with technical justification therefor, upon which these requirements have been established, and the evaluations required to show that safety functions will be accomplished. It is expected that reactors will reflect through their design, construction, and operation an extremely low probability for accidents that could result in the release of significant quantities of radioactive fission products. The descriptions shall be sufficient to permit understanding of the system designs and their relationship to safety evaluations. Items such as the reactor core, reactor coolant system, instrumentation and control systems, electrical systems, containment system, other engineered safety features, auxiliary and emergency systems, power conversion systems, radioactive waste handling systems, and fuel handling systems shall be discussed insofar as they are pertinent.

52.79(a)(ii) The extent to which generally accepted engineering standards are applied to the design of the reactor.

52.79(a)(2)(iii) The extent to which the reactor incorporates unique, unusual or enhanced safety features having a significant bearing on the probability or consequences of accidental release of radioactive materials.

52.79(a)(2)(iv) The safety features that are to be engineered into the facility and those barriers that must be breached as a result of an accident before a release of radioactive material to the environment can occur. Special attention must be directed to plant design features intended to mitigate the radiological consequences of accidents.

52.79(a)(4)(ii) The design of the facility including the design bases and the relation of the design bases to the principal design criteria.

Similar requirements to these are also included in 10 CFR 52.47 for Standard Design Certifications; 10 CFR 52.137 for Standard Design Approvals; and 10 CFR 52.157 for Manufacturing Licenses.

The use of Flibe salt environments is considered to represent a new and unique feature not typical of existing licensed light water reactor designs. The design and thermophysical properties of the KP-FHR reactor coolant enhances the safety of operations and reduces the probability of events [[ ]] . The design and thermophysical properties of the KP-FHR reactor coolant also provides additional functional containment protection, beyond that provided by the TRISO fuel particle, by absorbing fission products that escape the TRISO protective layer. This design feature reduces the probability of accidental release of radioactive materials. The specification limits and thermophysical properties of the reactor coolant for the KP-FHR are provided in the Kairos Power Topical Report, "Reactor Coolant for the Kairos Power Fluoride Salt-Cooled High Temperature Reactor" (Reference 6). This report describes the qualification and testing methods for the metallic structural materials in the high temperature Flibe salt environments for use in the Flibe-wetted areas containing safety-related high temperature components of the KP-FHR. As such, qualification of these materials using the methodology described in this report supports conformance, in part, to 10 CFR Part 50, Sections 50.34(a)(1)(ii)(C), 50.34(a)(2), 10 CFR 50.34(b)(4); and to 10 CFR Part 52, Sections 52.79(a)(2) and equivalent regulations in 52.47, 10 CFR 52.137, and 10 CFR 52.157.

1.2.2 Principal Design Criteria that are Relevant to the KP-FHR Material Qualification

Facilities licensed under 10 CFR Part 50 are also required to describe Principal Design Criteria (PDC) in their safety analysis reports supporting a construction permit and operating license application as described in 10 CFR 50.34(a)(3)(i). Likewise, applicants for standard design certifications, combined licenses, standard design approvals, and manufacturing licenses must include the PDC for a facility as described in 10 CFR 52.47(a)(3)(i), 10 CFR 52.79(a)(4)(i), 10 CFR 52.137(a)(3)(i), and 10 CFR 52.157(a).

The PDC for the KP-FHR have been established in the Kairos Power Topical Report, "Principal Design Criteria for the Kairos Power Fluoride Salt Cooled High Temperature Reactor" (Reference 7). The specific PDC in this report, which rely on or credit the design and performance of high temperature metallic structural materials include PDCs 14 and 31. These PDCs are discussed below.

The design and performance of high temperature structural alloys relates to conformance with PDC 14 because the materials used in the KP-FHR must ensure that they do not fail. The PDC states:

> *The safety-significant elements of the reactor coolant boundary are designed, fabricated, erected, and tested such that they have an extremely low probability of abnormal leakage, of rapidly propagating failure, and gross rupture.*

The design and performance of high temperature metallic structural materials is relative to demonstrating conformance to PDC 31 because the materials used in the KP-FHR must ensure that they are not unduly stressed under operating, maintenance, testing, and postulated accidents. PDC 31 states:

> *The safety significant elements of the reactor coolant boundary are designed with sufficient margin to ensure that when stressed under operating, maintenance, testing, and*

> *postulated accident conditions, (1) the boundary behaves in a nonbrittle manner and (2) the probability of rapidly propagating fracture is minimized. The design reflects consideration of service temperatures, service degradation of material properties, creep, fatigue, and other conditions of the boundary material under operating, maintenance, testing, and postulated accident conditions, and the uncertainties in determining: (1) material properties, (2) the effects of irradiation and coolant composition, including contaminants and reaction products, on material properties, (3) residual, steady-state, and transient stresses, and (4) size of flaws.*

Corrosion and Environmentally Assisted Cracking are important considerations for maintaining the integrity of the safety-significant portions of the reactor coolant boundary. Demonstration, through qualification, of the acceptability of the metallic structural materials used in the safety-significant portions of the reactor coolant boundary is a key element in establishing conformance to PDC 14 and PDC 31. The qualification requirements described in Sections 3 and 4 of this report, partially satisfy PDC 14 and PDC 31. A description of how the remaining portions of these PDC are satisfied will be provided in safety analysis reports submitted with licensing applications for the KP-FHR.

2 STRUCTURAL ALLOYS (INFORMATION)

2.1 BACKGROUND

Ductile, face-centered-cubic iron and nickel-based alloys (i.e., 'austenitic' alloys) are commonly used structural materials in light water reactors due to their combination of strength, toughness, and corrosion-resistance. Light Water Reactor (LWR) operation involves modest temperatures (215-345°C) but relatively high operating pressures (~7 MPa for BWR's and 16 MPa for PWR's). These temperatures translate into homologous temperatures (T_H)[1] of ~0.27-0.36 for the structural materials. These homologous temperatures are low enough such that solid state diffusion rates are slow and many degradation phenomena (e.g., alloy phase stability, creep, etc.) are of limited consequence.

Like LWR's, the KP-FHR (non-power test reactor and commercial power reactor) designs will use iron and nickel-based alloys for metallic structural components but at higher temperatures, lower pressure, and in different environments. Specifically, the design of safety-significant components of the KP-FHR reactors will use austenitic alloys at homologous temperatures [[ ]] in molten Flibe salt. These conditions require more consideration of high temperature material phenomena (e.g., thermal creep deformation) and, like water reactors, the molten salt coolants will require assessment for potentially susceptibility to Environmentally Assisted Cracking. For comparison, the approximate operating pressures and temperatures of LWR's, high temperature gas reactors HTGR's and sodium-cooled fast reactors (SFR's) and the KP-FHR is given in Figure 3. As shown, the KP-FHR will operate at significantly lower pressures than the BWR's, PWR's and high temperature gas reactors and at comparable pressures but somewhat higher temperatures than SFR's.

2.2 STRUCTURAL ALLOY SELECTION

The design of the KP-FHR reactor coolant boundary will be constructed from alloys qualified (or near qualification) by the ASME Code. Currently in ASME, Section III, Division 5, there are only a few alloys that are suitable for temperatures ≥ 600°C. These include the austenitic Alloys 304H, 316H, 800H, and 617. These four alloys have been assessed along with a modified version of Hastelloy N, the DOE developed Alloy 709, and the stainless-steel weld filler metal ER16-8-2 to both down-select candidate structural allows and to begin to identify any gaps in material availability or performance. These 7 alloys were ranked based on ten criteria:

- Status of ASME Code Qualification
- Mechanical and Physical Properties
- Experience with Molten Salts
- Experience in Nuclear Reactor Systems
- Technical Maturity
- Ability to Procure the Alloy in a Wide Variety of Product Forms
- Ease of Fabrication and Existence of a Matching Weld Filler Metal
- Environmental Compatibility of the Alloy with the KP-FHR Environments
- Degree of Regulatory Acceptance of the Alloy for use in Nuclear Systems

[1] Homologous temperature is defined as the temperature of interest divided by the melting point of the pure element that that alloy is based on in absolute units.

- Cost of the Alloy

A comparison of these rankings is provided in Table 2. As shown, the ranking for each category were assigned on a scale of 1 to 5 with a high rank (1 or a blue filled circle) being the most desirable and a low rank (5 or an open circle) being the least desirable. A summary of the factors that influenced eliminating the other structural alloys are provided below.

Alloy 304H is similar in composition and in many attributes to Alloy 316H. However, Alloy 304H displays notably lower allowable creep stresses at high temperatures. The benefits of Alloy 304H relative to Alloy 316H are few (e.g., marginally lower cost) and do not provide compelling reasons to select this alloy over Alloy 316H. Lastly, available data indicate higher corrosion rates for Alloy 304 as compared to Alloy 316 in Flibe (Reference 34). For these reasons, 304H was eliminated from consideration in favor of the more capable Alloy 316H.

Alloy 800H is often used in high temperature applications that require corrosion resistance. However, Alloy 800H is less creep-resistant than Alloy 316H and contains higher levels of chromium (~21 wt.% Cr vs. ~17 wt.%). Higher chromium levels are undesirable for corrosion-resistance in Flibe. Furthermore, Alloy 800H does not have a matching weld filler metal but is often welded with high chromium nickel-based alloys such as EN82H. The higher nickel in Alloy 800H/EN82 relative to Alloy 316H/ER16-8-2 is less desirable due to the potential transmutation of nickel to helium, which will adversely affect irradiation embrittlement. For these reasons, Alloy 800H is ranked lower than Alloy 316H stainless steel.

Alloy 617 was recently added to ASME Section III, Division 5 and possesses superior high temperature strength and creep resistance relative to Alloy 316H. However, the alloy contains a large amount of cobalt (10-15 wt.%) which can undergo undesirable neutron activation. The high strength of Alloy 617, while desirable, is not required for the low pressure KP-FHR design. Moreover, the attractive high temperature strength can present challenges when trying to hot-form the alloy and leads to fabrication challenges. Lastly, due to the expense and limited market for Alloy 617, it is only available in limited product forms.

Hastelloy N showed excellent corrosion-resistance in the MSRE experience but was susceptible to both tellurium embrittlement and degradation by irradiation (Reference 8 and 9). For this reason, a modified grade of Hastelloy N was considered in the rankings. However, Hastelloy N is not currently approved for use by ASME in high temperature reactors and modified grades are likely different enough composition (e.g., containing several weight % of niobium) to require a full ASME qualification effort. Furthermore, it is unclear what a suitable weld filler metal for a modified Hastelloy N would be. The lack of code qualification, lack of off-the-shelf commercial availability, and high costs associated with bringing a new alloy and a weld filler metal to market are major limitations that precluded selecting a modified grade of Hastelloy N.

Alloy 709 is an advanced stainless steel being developed by the DOE for nuclear power applications. While not ASME code qualified, this effort is in progress and to date, Alloy 709 displays a desirable combination of properties with higher creep strength than Alloy 316H as well as the potential for increased resistance to irradiation damage via alloy design. Notably, welding of Alloy 709 with a weld filler metal of the same composition indicates promising properties with weld degradation factors near 1. While the lack of current code qualification and industrial supply lowers the current ranking of this alloy, it may be considered for use in future licensing applications for the KP-FHR.

Alloy 316H and its weld filler metal ER16-8-2 possess a desirable combination of properties relative to the other candidate alloys. Alloy 316H is currently ASME code qualified, exhibits desirable mechanical properties, has demonstrated compatibility with Flibe salt, and has an extensive experience base in nuclear reactor applications. Furthermore, the alloy is technically mature with good availability, fabricability, and relatively low cost. The weld filler metal ER16-8-2 shows notable creep resistance and a high degree of weldability with Alloy 316H. Areas that require additional work for this alloy include extending the qualification of ER16-8-2 to higher temperatures (e.g., currently in the ASME code, the filler metal is limited to 650°C in the 2017 ASME Section III code), and additional research into the corrosion and environmental compatibility of these materials in Flibe. Based on this review, Alloy 316H/ER16-8-2 were selected as the metallic structural materials for safety-related components in the KP-FHR. These alloys were used as the basis for the expert panel PIRT review described in Section 4.1 which assessed environmental compatibility in Flibe salt. The remainder of the report is limited to the use and qualification of Alloy 316H/ER16-8-2 for safety-significant components in Flibe-wetted areas of the KP-FHR.

2.3 INDUSTRIAL EXPERIENCE WITH ALLOY 316H AND ITS WELD FILLER METALS

The following sections briefly describe the use of Alloy 316 in conventional nuclear reactors, advanced nuclear reactors, in non-nuclear but comparable high temperature industrial applications, and its compatibility with molten salt.

2.3.1 Conventional Nuclear Reactors

Austenitic stainless steels including Alloy 316 and Alloy 304, along with their weld filler metals, are commonly used for light water reactor internal components and corrosion-resistant cladding. Components made from these steels include fuel support structures, core barrels, flow baffle plates, and reactor vessel cladding. The low carbon variant of the alloy (i.e., the 'L' grade) is commonly used since high temperature strength is not limiting, but grain boundary chromium depletion (i.e., sensitization) is a concern. In light water reactors, grain boundary sensitization can result in intergranular corrosion and intergranular stress corrosion cracking if coolant chemistry is not maintained (e.g., if there is significant oxygen present in the coolant). However, Flibe salt is not oxidizing but highly reducing and its corrosion-resistance does not rely on the formation of a passive oxide film but on metallic stability in the salt. For stainless steels exposed to Flibe, the primary corrosion mechanism has been established as chromium loss (usually via grain boundary diffusion) to the coolant (Reference 10 and 11). Thus, sensitized microstructures are not inherently prone to corrosion but may be beneficial since lower chromium at the grain boundary results in less chromium lost via grain boundary diffusion.

In LWRs, irradiation can cause depletion of chromium and segregation of other elements at the grain boundaries of stainless steels and this combined with tensile stress can result in Irradiation-Assisted Stress Corrosion Cracking (IASCC) if the irradiation and stress levels are sufficient. For example, baffle-to-baffle bolts between the baffle plates in PWRs are susceptible to this degradation mechanism. However, the end-of-life irradiation doses for both the non-power test reactor and commercial power reactor are expected to be significantly lower than the dose threshold for IASCC susceptibility which is conservatively

taken as a neutron fluence of >3 dpa for PWRs with hydrogen water chemistry. Note that the KP-FHR reactors will see <0.1 dpa at end of life.

2.3.2 Advanced Nuclear Reactors

Austenitic stainless steels, including Alloy 316 have seen extensive experience in Sodium-Cooled Fast Reactors (SFRs) (Reference 12 and 13). In SFR's, austenitic stainless steels have been used throughout the primary plant with good experience. Analogous to corrosion in molten salt, when impurities in sodium such as oxygen and hydrogen are controlled to low levels, corrosion rates are low and are governed by alloying element solubility levels in the coolant (Reference 14).

While the nickel-based alloy Hastelloy N was chosen as the structural alloy for the MSRE construction, Alloy 304 and Alloy 316 were assessed in the MSRE program for their resistance to corrosion and to tellurium embrittlement (Reference 15, 16, and 17). In loop-type corrosion tests (i.e., tests with a hot leg and a cold leg) using Flibe salt at 650°C, these austenitic stainless steels exhibited corrosion rates ≤ 25 µm/year for short exposure times (<3000 hours) which decreased with time to ~8 µm/year after 3000-9000 hours exposure (Reference 16 and 17). Furthermore, when redox control of the salt was implemented (using Be metal additions), corrosion rates at 650°C were further reduced to levels estimated as <2 µm/year (Reference 16). While graphite can be a factor which increases corrosion rates, the data of Zheng et al., indicate this is a relatively modest ~2X increase in corrosion rate (Reference 18).

These results indicate that corrosion will be manageable for Alloy 316 components in the KP-FHR. For example, consider a thin-walled component such as a heat exchanger tube [[ ]] . Taking a reasonable, if not conservative corrosion rate of 2 microns per year (recall, Keiser et al., showed <2 µm/year (Reference 16) for Alloy 316 at 650°C in redox controlled Flibe) for a [[ ]] lifetime produces chromium loss to a depth of 0.04 mm (0.0016") or <4% of the wall thickness. It is important to note that this 0.04 mm represents a degraded layer (Cr loss), not a true reduction in wall thickness. In the chromium depleted layer, ~82% of the alloy remains (i.e., Alloy 316 is ~18 atomic % Cr).

In addition to manageable corrosion rates in Flibe salt, austenitic stainless steels also exhibit greater resistance to tellurium embrittlement than nickel-based alloys (Reference 19 and 20). The mechanism of tellurium embrittlement is well understood to be a result of the nickel – tellurium intermetallic formation (Reference 15, 21, 22, 23, and 24). Given the much lower nickel content of Alloy 316 compared to Hastelloy N, this intermetallic formation is less likely and a lower risk (Reference 25). Moreover, the KP-FHR design mitigates concern for tellurium embrittlement by the use of solid fuel and redox control of the salt (Reference 6). With the very low TRISO particle failure rate demonstrated in the DOE Advanced Gas Reactor program combined with the retention of tellurium in the fuel particle (Reference 26), the concentration of tellurium in the Flibe is expected to be significantly lower than the liquid fueled MSRE. Furthermore, the use of Be additions for redox control moves the electrochemical potential of the system away from the oxidizing regime of concern (Reference 6 and 15). For these reasons, concern for tellurium embrittlement in the KP-FHR are minimal.

2.3.3 Other Industrial Applications of Alloy 316

Austenitic stainless steels, including type Alloy 316H are used in a wide variety of high temperature industrial applications due to their corrosion-resistance, generally desirable mechanical properties, and wide industrial availability of product forms (Reference 27). For example, Alloy 316H, its welds, and similar austenitic stainless steels (Alloy 347 and Alloy 321) are used extensively in oil and gas refinery applications at temperatures and time frames of relevance to the KP-FHR (Reference 28 and 29). For example, petroleum refining applications of stainless steels include crude distillation, fluid catalytic cracking, delayed coking, hydrotreating, catalytic reforming, hydrocracking, gas plant, amine plant, sulfuric acid alkylation, and sour water stripper systems.

Furthermore, Alloy 316H and its weld metals are used in other industries near the time and temperature of the KP-FHR. Figure 4 illustrates the intended operation of the KP-FHR in the blue box ([[ ]] at 550°C-650°C), relative to the NIMS creep database (gray box) and selected high temperature, long life oil and gas refinery (Fluid Catalytic Cracking Units and Cyclone) components; the typical operating temperatures and service life of these components is estimated from (Reference 29 and 76). As shown, the KP-FHR is designed to operate at somewhat lower temperature and longer times than components in the oil and gas industry. However, it is important to note that (1) there is overlap in the time/temperature ranges of experience and (2) many oil and gas components operate at higher stresses and are limited by different environmental degradation phenomena than those of the KP-FHR. For example, Fluid Catalytic Cracking Units are typically exposed to strongly carburizing gaseous environments that can limit component life and rapid temperature cycles which generate appreciable thermal stresses (Reference 29 and 76). Neither condition is pertinent to the KP-FHR.

2.3.4 Compatibility with Molten Salts

In reducing salts, Alloy 316 is used in the pyro-processing of spent nuclear fuels. In that technology, chloride-based salts are used to convert oxide based nuclear fuel back to their metallic form (Reference 30, 31, and 32). In pyro-processing systems, austenitic stainless steels are used as structural alloys and generally display excellent corrosion-resistance as long as the salt is relatively free from oxidizing impurities (Reference 33). In addition to these industrial applications, there are significant laboratory data to support the use of Alloy 316 as a structural alloy in molten Flibe (Reference 16, 17, 18 and 34).

Some corrosion data for Alloy 316 in Flibe salt are shown in Figure 17, which shows corrosion depth versus time from Reference 18 and weight change versus time from the work of Keiser and Devan (Reference 16). As shown, the corrosion rate decreases with exposure time, likely with the square root of time as diffusional transport of chromium in the alloy limits the corrosion rate. As shown in the data of Zheng (top plot) the corrosion rates are on the order of ~80 µm/year at short exposure times (~1000 hours) and decrease with the square root of time (~21 µm/year at 6000 hours). Additionally, the work of Keiser shows the significant benefit of Beryllium metal additions, which effectively scavenge oxidizing impurities and reduce corrosion rates.

Austenitic stainless steel is also compatible with Flibe and graphite as shown by the work of Zheng et al. (Reference 18). Those researchers performed 1:1 experiments with and without graphite in Flibe at 700°C and showed about a modest increase in corrosion depth with graphite Figure 18 – top plot). Using the

Reference 18, data to compare predicted corrosion rates versus time, indicates graphite increases the corrosion rate approximately 2x (Reference 18). One way in which graphite likely increases the corrosion rate is by reaction with metallic chromium in the salt to form chromium rich carbides. Reaction of chromium ions in the salt to form carbides likely act to decrease the surface concentration of chromium and drive solid state diffusion. Note that in the corrosion testing programs proposed for the commercial power generation reactor and non-power test reactor, the test systems will incorporate large surface areas of graphite to capture these effects as detailed in Section 4.2.3.1.

3 AIR TESTING AND FINITE ELEMENT ANALYSES (INFORMATION)

For the design and licensing of KP-FHR reactors to the ASME code, high temperature material property data and subsequent analyses are desired. These testing and analysis efforts can be grouped as: (1) testing to extend the code qualification of ER16-8-2 weld metal up to [[ ]] to match the current qualification of Alloy 316H base metal and (2) testing and analyses required to support novel, high temperature design methods including elastic-plastic and inelastic design per the ASME Section III Division 5. [[

]]

3.1 TESTING REQUIRED FOR ASME CODE EXTENSION

ER16-8-2 weld filler metal is currently qualified up to 650°C in the ASME code while Alloy 316H is qualified to 816°C (Reference 37). The KP-FHR reactor vessel operates at approximately 550°C during nominal operations but could experience temperatures up to [[ ]] for short durations during postulated events [[

]] . Thus, an extension of the ASME Section III code qualification for ER16-8-2 up to [[ ]] . Mechanical testing of weldments will be required as described in the following paragraphs to develop a Code Case introducing stress rupture factors for Alloy 316 weldments with ER16-8-2 filler metal for temperatures between 650°C and [[ ]] .

The types of mechanical testing that are necessary to develop a Code Case for extending the stress rupture factors for Alloy 316 weldments with ER16-8-2 filler metal are described in ASME Section III Division 5, Non-Mandatory Appendix Y (Reference 37). The methods of testing that are required for such weldments as specified in Appendix Y are the ASTM E21 Elevated Temperature Tensile Testing, ASTM E2714 Creep-Fatigue Testing, and ASTM E139 Creep-Rupture Testing. In order to meet those requirements, the planned testing is detailed in Table 3 where the number in parentheses (X) indicates the number of test samples to be tested at that condition (i.e., (2) = two replicate tests).

The welds to support these tests have been fabricated utilizing Alloy 316H base metal[2] and ER16-8-2 weld filler metals, and the gas-tungsten-arc welding process. The Certified Material Reports for these materials are provided in Appendix F and Figure 20 shows that the composition of the weld filler metal (Heat 578409) is within ASME specifications. Two types of welds have been fabricated to support testing: (1) weld pad buildups and (2) v-groove weldments that use Alloy 316H siderails. Examples of these welds are provided in Figure 19. Note that the proposed Code Case to extend use of ER16-8-2 up to [[ ]] will be based on testing of a single heat (Heat # 578409 Lot YT0384) whose material certification is provided in Appendix F. This use of a single heat of material for a code case is consistent with ASME guidelines as described in HBB-Y-2300 which refers to ASME Section II, Part D, Appendix 5-1500. This article requires *"…(2) creep-rupture data for weldments made with one lot of consumables for each process intended to be used with the new base material."* The scope of the Code Case will limit the high temperature

[2] Note that all weld metal samples that are machined from weld pad buildups used Alloy 316L/316 base plates. The use of that material is appropriate since the samples machined far (>0.5") from the weld/base metal interface to mitigate any dilution of the weld metal composition. For samples that contain the base metal (e.g., cross-weld samples, other heat affected zone samples, the Alloy 316H plate was used.

applications to the Gas Tungsten Arc Welding (GTAW) process, which is the process used for fabricating the test specimens. Therefore, testing of a single heat of GTAW filler metal is sufficient to satisfy the ASME requirement.

Furthermore, these data will be assessed against larger sets of test data that encompass several heats of material to establish appropriate statistical confidence limits on the code case data. For example, a large database of ER16-8-2 weld metal was analyzed by ASME to develop a Larson Miller parameter equation for creep performance at temperatures up to 1200°F as described in ASME STP-PT-077 (Reference 40). A comparison of the ASME STP-PT-077 best estimate (solid) line and bounds (dashed lines) is given in Figure 21 which includes all available ER16-8-2 creep rupture data that has been found to date.

3.1.1 Elevated Temperature Tensile Testing

Elevated Temperature Tensile Testing was performed per ASTM E21 on all-weld-metal and cross-weld specimens at temperatures between 650°C and [[ ]] (1200°F – [[ ]]) at intervals of 38°C (100°F). These tests determined the 0.2% yield strength, ultimate tensile strength, % elongation, and % reduction in area at each temperature. The strength of the ER16-8-2 all-weld-metal at each temperature will be used to establish the creep-rupture and creep-fatigue test stresses. Note that data from these tests are available and are shown below in Figure 22. As shown, these data (triangles) are in good agreement with literature data on ER16-8-2 filler metal.

3.1.2 Creep-Fatigue Testing

Nonmandatory Appendix HBB-T of Section III, Division 5 provides a means to assess creep-fatigue of base metals, but it does not provide a dedicated means to assess creep-fatigue of weldments (Reference 37). Instead, the creep-fatigue analysis for base metals is applied to areas with welds and conservative restrictions are applied as follows (see HBB-Y-3400 of Reference 37);

> *"(a) limiting the inelastic accumulated strains to one-half the allowable strain limits for the base metal*
>
> *(b) limiting the allowable fatigue at weldments to one-half the design cycles allowed for the base metal*
>
> *(c) reducing the allowable creep rupture strength at weldments to a fraction of the base metal value through the weld strength rupture factor when determining time-to-rupture."*

Creep-Fatigue testing per ASTM E2714 of all-weld-metal and of cross-weld specimens is performed only to verify the adequacy of the HBB-T treatment of weldments (Reference 38). If the restrictions specified in HBB-Y-3400 bound the ASTM E2714 creep-fatigue test data, then the Non-mandatory Appendix HBB-T analysis procedures for base metal with specified restrictions for welds will have been determined to be adequate for creep-fatigue analysis of welds.

3.1.3 Creep-Rupture Testing

Creep-Rupture tests will be performed in accordance with ASTM E139 (Reference 39). The time, temperature and load conditions for the creep-rupture tests are derived from design Service Level conditions. ASME Section III Division 5 HBB-Y-2200 allows creep-rupture curves to be extrapolated up to a factor of five from the maximum creep-rupture test duration. The maximum operating service time at each temperature is therefore divided by 5x to determine the approximate maximum test duration to assess the component life. For example, for a 100,000-hour service lifetime, a minimum test duration of 20,000 hours is sufficient to bound the operating life. The test duration and temperature can then be inserted into the appropriate creep correlation (e.g., the Larson-Miller model) to estimate the test load that will be required to produce specimen rupture at each specified time and temperature combination (Reference 40).

Testing will be performed on both all-weld-metal ER16-8-2 specimens as well as on cross-weld specimens. The rupture strength of the weld metal will be divided by the rupture strength of the base metal at each time and temperature combination to determine proposed stress rupture factors. An ASME Code balloting plan will be developed and the proposed rupture factors and supporting data will be presented to the relevant ASME Code Committees for review and approval. Progress on this extension is presently being tracked through ASME Codes & Standards Record #19-2745. Once the Code Case has been approved by ASME, then it will be presented to the NRC for approval. Once approved by the NRC then the stress rupture factors at the higher temperatures will be used in the same manner as those at the lower temperatures to determine the allowable stresses for specific temperature and time durations.

3.2 TESTING TO FACILITATE NON-POWER REACTOR AND COMMERCIAL POWER REACTOR DESIGNS

To facilitate design via the ASME Section III, Division 5, additional test data are required to calibrate and validate ASME design methodologies. A testing program to extend the qualification of the weld metal to higher temperature for the non-power and commercial power reactor designs was presented in the previous section and Table 3. For Alloy 316H stainless steel model calibration and validation that will be used for the non-power and commercial reactors, six types of tests will be performed in air: (1) tensile tests, (2) stress relaxation tests, (3) strain rate change tests (aka ‘stress dip’ tests), (4) uniaxial creep rupture, (5) notched bar creep rupture testing (aka ‘3D creep tests’) and (6) creep-fatigue testing.

3.2.1 Tensile Testing

[[

]]

3.2.2 Stress Relaxation Testing

[[

]]

3.2.3 Stress Dip Testing

[[

]]

3.2.4 Uniaxial and Notched Bar Creep Testing

[[

]]

3.2.5 Creep-Fatigue Testing

Creep-fatigue tests are listed in Table 9.

3.3 HIGH TEMPERATURE TESTING & ANALYSIS TO SUPPORT POTENTIAL DEGRADATION

As part of the Phenomena Identification Ranking Table (PIRT) process detailed in Section 4.1, some degradation phenomena (or factors that influence degradation phenomena) that are primarily driven by temperature were identified. These were: (1) degradation via stress relaxation cracking, (2) weld residual stresses, (3) other thermal stresses from operation, and (4) thermal striping. Since those issues can be addressed via testing in air (and/or via modelling), they are addressed below.

3.3.1 Stress Relaxation Cracking

Cracking of austenitic stainless steels in the temperature range (approximately 500-700°C), aka 'stress relaxation cracking' has been a concern since the 1950's (Reference 77, 78, and 79). In general, alloys of greatest concern have been the stabilized grades 347 and 321 (Reference 77, 78, 80, and 81) although types 304 and 316 stainless steel can be susceptible under conditions which produce high triaxial stresses (Reference 78, 79, 82, 83 and 84) as noted by research of Spindler et al. (Reference 86, 88 and 89).

While stress relaxation cracking of weld metal has been reported in chrome-moly steel and 347 weld metal (where Nb(C,N) precipitation leads to susceptibility), types 16-8-2 and 316 weld filler metals are noted for their resistance (Reference 78 and 79). To date, a literature search has not revealed any reported cases of reheat or stress relaxation cracking occurring in ER16-8-2 weld metal. Instead, the concern for Alloy 316H / ER16-8-2 appears to be limited to the heat affect zone and in components that are subjected to appreciable triaxial stress (Reference 79, 87, 89 and 90).

Several approaches are used to mitigate the risk of stress relaxation cracking. These include:

- The use of Alloy 316H base metal, which is noted to be more resistant to stress relaxation cracking than the stabilized grades, as well as the use of ER16-8-2 weld filler metal, which has not been observed to exhibit stress relaxation cracking.
- Design of welds and application of welding processes and parameters which are resistant to stress relaxation cracking. Lower triaxial stresses are known to be beneficial for decreasing the risk or severity of stress relaxation cracking. For example, the bottom head to shell weld utilizes a machined weld preparation to move the weld joint from the notch formed by the shell / bottom head interface up into the shell which minimizes the triaxial stresses (Figure 23).
- Developing the capability to model weld residual stresses and to better assess the risk of any weld joints for stress relaxation cracking if needed, and
- Experiments for the non-power test reactor testing will assess the bounding triaxiality allowed by the ASME code for both Alloy 316H and Alloy 347 heat affected zones to (1) assess if this type of cracking can be triggered in Alloy 316H and (2) to compare the relative resistance of these two austenitic stainless steels. This testing will be followed by an additional study for the commercial power reactor as detailed in Table 10.

These tests follow the work of Spindler and Smith, who have used notched tensile bars to assess the effects of triaxiality and temperature on susceptibility to stress relaxation cracking (Reference 46). [[

]]

[[

]]

3.3.2 Weld Residual Stresses

Weld residual stresses are known to influence some environmental degradation phenomena like stress corrosion cracking. [[

]]

3.3.3 Thermal Stresses & Thermal Striping

[[

]]

4 COMPATIBILITY WITH FLIBE AND IRRADIATION (APPROVAL UNLESS NOTED)

As noted above, Alloy 316H is already an acceptable material for use in high temperature reactor applications in ASME Section III. However, the code requires demonstration of the environmental and irradiation compatibility of the structural materials. For the KP-FHR safety-related systems, the environments of interest include high temperature air (external to the system) and molten Flibe salt (internal to the system), with exposure to neutron irradiation.

4.1 REVIEW OF POTENTIAL ENVIRONMENTAL AND IRRADIATION ISSUES

Due to the breadth and complexity of environmental issues, an expert panel consisting of experts from national laboratories, universities and consultants was convened to assess potential environmental issues for Alloy 316H / ER16-8-2 in each of the KP-FHR heat transport loops. This review was performed for a KP-FHR power generating reactor assuming a [[ ]] operational life and a secondary coolant loop that uses a different molten salt than the primary coolant loop. Based on this review, a full set of tests for the commercial power reactor was defined. A subset of tests was also developed for the lower power, shorter lifetime, non-power test reactor.

This review utilized a process based on the Phenomena Identification and Ranking Table (PIRT) methodology in NRC Regulatory Guide 1.203. Only the environmental degradation issues pertinent to potential safety-related components (exposed to Flibe and air) are summarized in this report. Component materials degradation considerations are summarized in Figure 6, which presents the Venn Diagram for the Material – Stress/Strain – Environment degradation phenomena of concern for the expert panel.

In total, there were 23 degradation phenomena assessed by the expert panel in 7 unique systems, structures, and components (SSC's). This resulted in 198 scenarios assessed by the expert panel to start, with ten scenarios added during the PIRT for 208 total rankings. Each scenario was ranked based on its importance (high, medium, low) and the degree of knowledge (high, medium, low). The PIRT rankings are shown schematically in Figure 7. Phenomena with high importance and low knowledge are the greatest priority (upper right box), followed by phenomena with high importance and medium knowledge (upper center box) and phenomena with medium importance but low knowledge (middle right box). These categories are given a numerical ranking, where Category #1 indicates that highest priority phenomena to investigate (high importance and low knowledge), Category #2 is the next important, etc. Note that each degradation phenomenon was ranked so that a total of seven, equally weighted rankings were used to develop average knowledge and importance levels.

In considering the results of the review, a conservative approach was adopted to determine which phenomena warranted future investigation. Rather than take an average ranking, phenomena were considered based on if any Expert gave it a ranking of 1 (High Importance / Low Knowledge), 2 (High Importance / Medium Knowledge), or 3 (Medium Importance / Low Knowledge). Results from those rankings are given in Figure 8. The excluded phenomena are of such low importance or high knowledge as to not warrant further consideration.

In Figure 8 the open symbols identify phenomena that will be addressed by further investigation while the 'X' symbols show the low ranking of the phenomena that will not be addressed. The degradation

concerns that warrant further investigation are grouped into categories with corrosion related phenomena being identified by blue circles, environmentally assisted cracking by green squares, 'other' phenomena by gray triangles and irradiation effects by red diamonds.

The resulting phenomena to be further addressed are presented in Table 11, which summarizes the issues. Note that Table 11 only presents the degradation phenomena for safety-related components. The degradation phenomena are grouped into four categories: corrosion, environmentally assisted cracking, 'other' phenomena, and irradiation effects. For each category, the phenomenon of interest is listed along with a brief description and major variables that additional investigation will address.

Given the materials testing categories in Table 11 (Corrosion, Environmentally Assisted Cracking, Metallurgical Phenomena, and Irradiation Effects), the following sections outline the testing and modelling that will address those concerns. These efforts support appropriate design, operation, and inspection requirements for a [[ ]] of the structural materials. Unless otherwise noted, all tests will be performed on the base materials (Alloy 316H that meets ASME Section III Division 5 compositional requirements) and on the weld filler metal (ER16-8-2).

4.2 ENVIRONMENTAL COMPATIBILITY

4.2.1 Use of the PIRT Data for NRC Licensing

The PIRT review, which identifies and ranks the appropriate environmental degradation phenomena that are applicable to safety-related components of the KP-FHR (i.e., the reactor vessel which serves the function of retaining the coolant around the fuel) was completed.

[[

]]

Note that the environmental testing described below is targeted to satisfy PDC 31 for safety-related components (i.e., the Flibe-wetted reactor vessel and reactor vessel internals) which operates at approximately 550°C during normal operation and is expected to see higher temperature transients infrequently and for short time periods. To address a large range of potential operational transients as well as many accident scenarios, testing between 550-750°C and environmentally assisted cracking testing between 550-750°C is planned to be conducted. [[ ]]

[[

]] A summary of the results of transient safety analyses will be provided in the application for an operating license.

In addition to testing at or above the normal operating temperature of the reactor vessel, many of these tests encompass other aggressive testing conditions such as the use of 'Nominal' Flibe salt rather than redox controlled Flibe or high applied stresses and stress intensity factors relative to what the reactor vessel is expected to see. [[

]]

The PIRT identified two potential accident scenarios (for the commercial power reactor) that could affect the safety-related components, i.e., air ingress and intermediate coolant ingress into the Flibe salt. Note that the KP-FHR technology mitigates these concerns via design features. For example, air ingress is prevented via the hermetically sealed containment and the use of an inert gas overpressure in the reactor vessel. Similarly, intermediate coolant contamination of the Flibe is prevented via the design of the intermediate heat exchanger and by operating the Flibe at a higher pressure than the intermediate heat exchanger. Testing to better assess the effects of air and intermediate coolant contamination of the Flibe as detailed below in Section 4.2.3.3 is planned. Note that the non-power test reactor system uses a Flibe-to-air heat rejection subsystem.

A third potential accident scenario, water ingress into the Flibe has been discussed but judged not to be credible for the following reasons. There are two potential sources of water near the reactor vessel, a cavity cooling system and a decay heat removal system. Both these systems contain design features such that water ingress into the Flibe is not a credible accident scenario as described below.

The potential location of the cavity cooling relative to the reactor vessel is shown schematically below in Figure 25. As shown, cavity cooling is planned to be inside the concrete cavity wall and further separated from the reactor vessel via a steel liner. Given these design features, failures in the cavity cooling do not have a credible path to cause water ingress into the reactor vessel or heat transport system Flibe in any credible operational or event scenario.

Similarly, the decay heat removal system uses multiple design features to preclude any contact with the reactor vessel or Flibe salt. The decay heat removal system is planned to use two barriers to prevent leaks into the reactor cavity. The first barrier is the primary heat transport system piping and reactor vessel physical boundary. Outside of that there is a second wall. The intervening gas space humidity is monitored to check for leaks in the primary heat transport piping. This prevents Flibe-water interaction in two-ways:

(1) leaks from the decay heat removal system would be identified sufficiently early to shut down the system and replace components as necessary before bulk water can enter the reactor cavity.

(2) The outside barrier would act to protect the decay heat removal system piping from the thermal shock associated with Flibe spraying on it. The external barrier used for leak checking prevents direct spray on

the decay heat removal system, which inhibits bulk-interaction between water and Flibe. Both barriers must fail before bulk interaction may occur.

4.2.2 Alloys and Heats to be Assessed

Potential heat-to-heat variability in environmental testing was identified in the PIRT. For the known degradation of austenitic stainless steel exposed to fluoride salts, the primary issue is loss of chromium from the grain boundaries to the salt. This grain boundary chromium loss has not exhibited heat-to-heat sensitivity but is fundamentally controlled by the solid-state diffusivity of chromium, a process that is not sensitive to minor changes in alloy composition. For example, recent evaluations show very similar corrosion rates between dual certified 304L/304 stainless steel in Flibe and 316L/316 stainless steel and with a fundamentally based prediction as shown below in Figure 26.

[[

]]

[[

]]

4.2.3 Corrosion

Corrosion tests of prototypic materials to develop quantitative corrosion rate models for Flibe will be conducted. [[

]]

4.2.3.1 Testing Systems

[[

]]

[[

]]

[[

]]

[[

]]

4.2.3.2 The Use of Compositional Analysis and Electrochemical Potential (ECP) Monitoring

Both compositional analysis of the salt and ECP monitoring are planned. [[

]]

[[

]]

[[

]]

[[

]]

[[

]]

[[

]]

[[

]]

[[

]]

4.2.3.3 Corrosion Testing

The planned corrosion testing is summarized in Table 12 which gives the purpose of the test, the materials to be tested, the environment and the approximate test temperatures and duration. For each test, the depth of chromium loss will be assessed over time to establish the governing corrosion kinetics (Equation 1) and to establish the steady state corrosion rate. Note that while the weight change of each corrosion coupon will be documented, the analytical electron microscopy is intended to be used to determine the extent of corrosion or other metallurgical changes (e.g., Cr loss depth, carbide precipitation, etc.). Additional details of the corrosion testing and an example of the planned statistical analysis of the data are provided in Appendix C.

The purpose of each test is further elaborated in Table 13 and discussed below. For most tests, the corrosion rate will be established by assessing the depth of chromium loss from the sample surface. The chromium loss depth will be determined by an appropriate analytical technique such as wavelength dispersive spectroscopy. In addition, the weight change of the corrosion coupons will be determined. The following bullets expand on the purpose of each test.

$$Cr\ loss\ depth \propto \left(t, \sqrt{t}, log\ t, \frac{1}{log\ t} etc.\right) \qquad \text{Eq. 1}$$

- Temperature: The testing as a function of temperature in nominal Flibe for Alloy 316H and ER16-8-2 will determine the corrosion rate for each alloy and will be used as a baseline to judge subsequent separate effects testing. At each of the three planned temperatures, tests will be conducted for different times to determine the controlling kinetics and the steady state corrosion rate. The steady state rates will then be used to develop best-estimate and design-estimate predictions of corrosion rate as a function of temperature. These data will be fit to a model of the form of Equation 2 and provide a standard against which the separate effects tests described below can be quantitatively judged.

$$Corrosion\ Rate = A \cdot \sqrt{\mathrm{t}} \cdot EXP\left(-\frac{Q}{RT}\right) \qquad \text{Eq. 2}$$

- Microstructural Effects: The effects of the weld heat affected zone, long-term thermal aging, and cold work (20% via rolling) will be assessed and compared to the baseline (temperature dependent models). [[

]] This testing has been eliminated since a post weld heat treatment will not be utilized.

- Salt Composition: The salt composition testing will assess the effects of the impurities and redox control. The impurity testing will cover accident scenarios defined in the materials PIRT review: nitrate ingress for 168 hours and air ingress for 168 hours (i.e., scenarios 3 and 4). The conditions of the accident scenarios have not been defined at this time and will be provided in safety analysis reports submitted with a future license application. These tests will determine the effect of

potential loss of salt chemistry control on the corrosion rate. Redox control will be investigated via separate effects testing in order to define a factor of improvement in corrosion rate relative to the nominal Flibe purity.

- Occluded Geometry: The intent of these tests is to investigate if a physical crevice influences the corrosion rate with and without redox control of the salt. Occluded geometry will exist on all corrosion samples due to small gaps between samples and the sample cage of RCL systems. The nominal aspect ratio of this crevice is 12 (width/depth) and the minimum aspect ratio is 3.17, based on fabrication tolerances. For a subset of samples, these creviced surfaces will be characterized and compared to fully exposed surfaces. Additionally, unloaded, pre-cracked reference samples used in SCC testing will be used to further evaluate occluded geometry effects. These reference samples will be fitted with an insert which creates long crevices. Note that screening work at ORNL on a nickel-based alloy indicates that crevice corrosion is not a concern in fluoride salt (Reference 87).

- Erosion-Corrosion and Graphite Contact: These tests will assess the potential effect of erosion-corrosion. Specifically, graphite particulate will be introduced into corrosion tests with flow to assess if hard particles (e.g., potentially from the graphite reflector) will significantly impact corrosion rates. In these tests, weight change of the coupon (via chromium loss depth) will be used as the primary indicator of the corrosion rate.

- Cold Leg Occlusion: In addition to the effect of temperature on the corrosion rate (hot leg samples), many of these tests described above will be used to assess the potential for cold leg occlusion. Cold leg occlusion will be assessed by monitoring the flow rate of salt circulating between hot and cold legs. This rate is estimated using heat flow analysis and furnace power inputs. Additionally, RCL systems will be inspected during planned shutdowns for sample exchanges, and during decommissioning and teardown to look for evidence of cold leg occlusion.

4.2.3.4 Discussion of Redox Control and Monitoring Test Systems

[[

]]

[[

]]

4.2.4 Environmentally Assisted Cracking

Literature data for environmental degradation of both stressed and unstressed samples were recently reviewed in Reference 42 and updated in Table 20. In general, there has been little mechanical testing in molten salts and few data of relevance to the KP-FHR. In part, this is due to the difficulty of conducting in-situ mechanical testing in highly reducing molten salt.

Relatively little literature data exists for structural alloys undergoing environmentally assisted cracking in molten salts. Fluoride salts are of primary interest to the KP-FHR technology and Table 20 summarizes literature studies of EAC in molten fluoride salts. For the 10 studies shown, 7/10 are for Ni-Mo-Cr family of alloys (INOR-8 / Hastelloy N or variants) that were used in the Molten Salt Reactor Experiment (MSRE), while only two studies investigate austenitic stainless steels and there is one report of EAC in oxygen free high conductivity (OFHC) copper based on post-operation examination of the MSRE.

Evidence for intergranular stress corrosion cracking of the OFHC copper component was clear but the precise environmental and mechanical conditions that produced the cracking were not. This observation was from the post-irradiation examination of materials from the MSRE where a cup used to take salt samples was inadvertently lost, plastically deformed during attempts to retrieve it, and subsequently exposed to fuel salt for ~13,000 hours (Reference 9). The cup was recovered post-operation and showed extensive intergranular cracking and the copper was noted to be brittle. Compositional analyses via the electron microprobe and mass spectrometry indicated that the copper alloyed with nickel with local regions enriched in chromium and molybdenum, including a grain boundary second phase that was rich in chromium. No conclusions were reached as to the causes of the brittleness of the OFHC copper (Reference 9).

More extensive research into environmental compatibility of the structural alloy INOR-8 (Hastelloy N, Ni-16Mo-7Cr-4Fe) was also part of the Aircraft Reactor Experiment (ARE) and the subsequent MSRE programs. The mechanical properties of several heats of INOR-8 exposed to the ARE fuel salt 11.2NaF-41KF-45.3LiF-2.5UF4 (mol %) were reported by Swindeman (Reference 97). In that work, tensile tests, creep tests, and stress relaxation tests were performed in both air and the fuel salt. It is notable that in creep testing, the fracture mode of the alloy was often intergranular in both salt and in air but creep rupture ductility was sufficiently high (often ~6% elongation when tests were conducted to failure) such that no environmental degradation in salt was noted (Reference 97). It is interesting to compare these results with the more recent research of Shrestha et al. on a similar Ni-16.0Mo-6.4Cr-3.6Fe alloy (Reference 98). In those creep rupture tests performed in both air and in FLiNaK salt at 700°C, there was clear evidence of environmental degradation with the salt exposed samples exhibiting ~50% shorter

failure times and extensive intergranular cracking. Notably, the creep failure strains in both environments were high with failure occurring ~20% strain in FLiNaK and ~50% strain in air. The mechanism of the degradation in the FLiNaK was suggested to be preferential corrosion of molybdenum depleted grain boundaries (Reference 98).

One mechanism of EAC discovered in the MSRE program that has garnered some additional research is the embrittlement of nickel-based alloys by tellurium (and similar Group 16 'Chalcogen' elements) and similar elements (Se, S, etc.) (References 9, 15, 20, 22, 23, 24, 99, 100 and 101). In laboratory testing, intergranular cracking via tellurium embrittlement was noted in several nickel-base alloys (Hastelloy N, Hastelloy S, Inconel 600) but not in Alloy 304 stainless steel (Reference 20). Under conditions where tellurium is plated on the surface of the alloy (oxidizing potentials), it preferentially diffuses down fast paths like grain boundaries and forms brittle intermetallic compounds (e.g., Ni_3Te_2, CrTe, $MoTe_2$, etc.) that cause intergranular cracking (References 23, 24, 102 and 103). Iron-based alloys such as 304 stainless steel appear to be more resistant to this type of embrittlement, in part due to the lesser tendency to form the Ni and Mo – rich intermetallic phases. Embrittlement of Ni-Mo-Cr alloys (INOR-8 / Hastelloy N) can be mitigated via alloying with ~1-2 wt.% niobium, which is believed to slow Te grain boundary diffusion (Reference 20). However, alloying with both Nb and Ti was shown to negate the beneficial effect of niobium (Reference 20). In addition to the embrittlement produced by intermetallic formation, first-principles work indicates that tellurium, like sulfur, also causes intrinsic grain boundary Ni-Ni bond weakening and likely promotes grain boundary decohesion (Reference 104, 105 and 106).

Environmental degradation of nickel-based alloys via sulfur embrittlement was noted in mechanical testing (Reference 99) during salt processing (Reference 25) of the MSRE program. These observations showed (1) intrinsic embrittlement of nickel or nickel alloy grain boundaries by sulfur as show by high temperature exposure and low temperature testing and (2) cracking due to the formation of the low melting point Ni_2S eutectic. In mechanical testing of Hastelloy N, exposure to a sulfur rich environment resulted in a degradation of both the tensile and creep performance of the alloy (Reference 99). Similarly, impure Flibe salt has been noted to cause cracking of nickel alloy processing and testing equipment (e.g., a salt transfer line), likely through the formation of a low melting eutectic (Reference 25 and 107). Iron based alloys like austenitic stainless steel are notably more resistant to the development of sulfur rich eutectic compositions with the lowest melting Fe-S eutectic forming approximately 1027°C while Ni_2S forms approximately 636°C.

The MSRE program also performed limited testing of austenitic stainless steels which were shown to be more resistant to both tellurium embrittlement and degradation by sulfur than INOR-8. However, austenitic stainless steels contain more chromium than INOR-8 (~17 wt.% vs. ~7 wt.%) which can result in faster corrosion rates under oxidizing conditions. An in-situ mechanical testing system was developed to support additional investigation of this phenomena which is shown schematically in Figure 32. Key features of the testing systems include:
[[

]]

The in-situ mechanical testing systems will be used to conduct the slow strain rate, corrosion fatigue, stress corrosion cracking, and in-situ creep testing described below.

4.2.4.1 Slow Strain Rate Testing

Slow strain rate testing (SSRT) will be conducted in nominal Flibe to assess if Alloy 316H, ER16-8-2, and the heat affected zone of Alloy 316H are susceptible to environmentally assisted cracking in fluoride salts. The SSRT is a well-established and accepted methodology to determine susceptibility to stress corrosion initiation and crack growth (Reference 43). Testing will be conducted in accordance with ASTM guidelines outlined in ASTM G129-00 (Reference 44). The SSRT tests will be conducted on flat, pin-loaded specimens. Tests will be conducted at three different temperatures 550, 650, and 750°C, at four (4) strain rates between $1x10^{-6}$ - $5x10^{-8}$ (in/in)/sec as detailed in Table 14. Note that the 750°C tests will be run only at faster stroke rates, consistent with potential accident scenarios. In the tests, the degree of an environmental effect will be assessed by comparison of the load/stroke curves with comparable tests conducted in air as shown schematically in Figure 10. Additionally, the fracture mode of these test samples will be investigated to better assess any potential environmental damage. For the non-power test reactor, only heat affected zone samples will be tested. These samples contain all three materials of interest (weld metal, Alloy 316H heat affected zone, and unaffected Alloy 316H) within the gauge section of the tensile bar and are judged to be an efficient method to assess EAC susceptibility.

4.2.4.2 Fracture Mechanics Based Testing: Corrosion Fatigue and Stress Corrosion Cracking

In addition to the slow strain rate testing, fracture mechanics-based testing will be performed on pre-cracked samples based on established methods (Reference 45). These tests will assess prototypical materials (Alloy 316H and ER16-8-2 weld filler metal and the Alloy 316H heat affected zone) and be conducted in nominal Flibe and redox controlled Flibe as provided in Table 15. These tests will include both a corrosion fatigue portion of the test and a constant stress intensity factor portion of the test to assess stress corrosion cracking. The corrosion fatigue portion of the test will initially be at relatively high ΔK's to produce fatigue crack growth and will subsequently shed load to both (1) determine the 'Stage II' Paris-law crack growth rate and (2) to prepare the sample for subsequent stress corrosion cracking testing.

These in-salt fatigue crack growth rates will be compared to similar data determined at temperature but in-air to assess any potential degradation, e.g., the difference between in-air vs. in-salt behavior. Example corrosion fatigue data and their comparison to air data are shown in Figure 11. At the completion of the corrosion fatigue portion of the testing, constant stress intensity factor (K_I) testing will be conducted.

[[

]]

[[

]]

The intent of the constant *K* portion of these tests is to attempt to initiate stress corrosion under aggressive testing conditions and then transition to conditions that are more representative of the KP-FHR. For the non-power test reactor, only tests on heat affected zone samples will be tested. In these tests, the sample notch will be machined in the heat affected zone of the sample. A sharp flaw (i.e., the corrosion fatigue crack) is placed near the microstructures of interest (weld metal, HAZ and base metal) and allows the crack to grow in the region of highest susceptibility. This methodology has been applied in other EAC testing where intergranular stress corrosion cracking was shown to occur preferentially in the HAZ in samples of EN82/A600 HAZ/A600 (Reference 109). These tests will be followed up by dedicated tests of the base metal and the weld metal as provided in Table 15. One potential SCC mechanism (strain accelerated corrosion and subsequent intergranular cracking) and how its stress corrosion rates may evolve are provided in Figure 12.

4.2.4.3 Environmental Creep Testing

The potential for environmental degradation during creep loading will be assessed for environmentally assisted cracking. For the non-power test reactor, the potential for environmentally affected creep rates will be assessed by comparing SSRT data from air to SSRT data in both nominal Flibe and redox controlled Flibe. The SSRT tests incorporate creep effects during deformation as evidenced by changes in the flow curve as provided in Figure 10 (References 110 and 111).

For the commercial power reactor, creep testing in Flibe will be conducted as indicated in the baseline testing plan.

Creep-rupture testing in Flibe for the commercial power reactor will be conducted to further assess the compatibility of Alloy 316H, ER16-8-2 filler metal, and the Alloy 316H weld heat affected zone with the molten salt. This testing will target creep rupture times on the order of 500 hours and 2000 hours. The creep tests will be conducted at 550°C and 650°C in nominal Flibe and will assess the integrated effects of environment and stress on the materials performance. Additionally, a short time 750°C test will be conducted to cover potential accident scenarios. The stress is lower based on the higher test temperature (750°C). A pressure of 83 MPa corresponds to the best estimate 200-hour creep rupture life for 316H plate at 750°C from the Japanese NIMS Database. 'Cross weld' samples will be used such that the gauge section of the creep sample contains both base metal, heat affected zone and weld metal to best assess a range of materials and microstructures. These creep rupture times will be compared to data from air tests to determine any reduction in creep rupture lifetime due to the salt. Also, the samples will be characterized for chromium loss and compared to unstressed corrosion coupons. The targeted environmental creep test conditions are given in Table 16. Note that replicate tests will only be conducted if significant degradation is observed, e.g., a failure time outside of the 90% confidence interval for air test data and/or if a change in fracture mode is observed.

4.2.5 Metallurgical Effects

The potential environmental degradation phenomena grouped into the 'other' category were stress relaxation cracking, phase formation embrittlement, and degradation driven by thermal cycling or by thermal gradients. Each of these phenomena will be addressed to assess the risks of each phenomenon for Alloy 316H. Assessing stress relaxation cracking involves testing in air and as discussed in Section 3.3.1 further analysis and design changes indicate that the risk of this phenomena is sufficiently low such that additional testing is not required.

Testing for phase formation embrittlement addresses the concern that some element could be picked up by the stainless-steel during exposure to Flibe (e.g., carbon or beryllium) and form a deleterious second phase. For example, near-surface carbide precipitation in Alloy 316 exposed to Flibe+ graphite has been noted by Zheng et al. (Reference 18). Similarly, when beryllium metal is coupled to nickel, iron, or stainless steel and exposed to elevated temperature, Be can diffuse into the other metal and can exacerbate corrosion rates (Reference 48). When excess Be is present in nickel, iron or similar alloys, Ni-Be precipitates can form and increase corrosion rates, possibly by generating internal stress (Reference 48 and 49). [[

]] These samples will include at least one SSRT sample (for the non-power test reactor) and one in-situ creep sample (for the commercial power reactor) as detailed in Table 17.

Lastly, degradation of materials can be driven by thermal phenomena that are influenced by the environment. For example, poor mixing in the coolant could lead to local temperature gradients and result in unwanted thermal stresses (thermal striping). Similarly, the large thermal transients associated with draining and/or filling the reactor vessel could result in 'ratcheting' of the pressure vessel. However, several design features and the high Prandtl number of Flibe act to reduce the magnitude of thermal stresses (Reference 50). These phenomena are considered to be appropriately addressed via analysis and specific concerns can be mitigated via design and operational procedures without the need for testing.

4.2.6 Irradiation Effects

The PIRT review identified three irradiation-influenced phenomena that may warrant additional work; irradiation-induced embrittlement, irradiation affected corrosion, and irradiation assisted stress corrosion cracking (IASCC). The following sections describe the additional investigation activities to address irradiation effects. The results of these efforts are to establish the appropriate design, operation, and inspection requirements for the non-power test reactor and the commercial power reactor systems. The expected reactor vessel irradiation damage and helium generation are compared in Table 21. While current estimates for the displacement damage are estimated at <0.1 dpa for both reactors, the shorter-lived non-power test reactor will generate less helium that the longer-lived power reactor. A more detailed evolution of the displacement damage and helium generation for the commercial power reactor is provided in Figure 13.

4.2.6.1 Irradiation-Induced Embrittlement

The existing published data on austenitic stainless steels indicate that tensile properties at temperatures from 550°C to 650°C are relatively unaffected by <0.1 dpa and ~10 appm of He when tested at moderate or high strain rates (>$10^{-3}s^{-1}$). For example, a compilation of tensile data in Reference 51 indicates virtually no change in yield strength or tensile elongation ≤0.1 dpa for several austenitic stainless steels, including Alloy 316 variants. Similarly, fracture toughness remains high in austenitic stainless steels below 0.1 dpa, with values in excess of 100 MPa√m (Reference 52). While most fracture toughness studies focus on LWR conditions (Figure 14), those data indicate that fracture toughness remains high at ~0.1 dpa. Work by Bernard on Alloy 316H (Reference 53) and DeVries on Alloy 304 (Reference 54) at 550°C confirm that fracture toughness is high at conditions of the KP-FHR operation with J_{IC} values near 100 kJ/m^2. In Figure 14, the apparent increase in toughness at 0.3 dpa may be due to some irradiation-induced hardening before any appreciable loss in ductility, which is reasonable based on the tensile data of Nagae (Reference 51).

However, when testing at low strain rates, irradiation-induced embrittlement is clearly a concern where structural alloys are known to exhibit helium embrittlement. An example study of the effect of strain rate and temperature on ductility of an austenitic stainless steel is shown in Figure 15 (Reference 55). As shown in Figure 15, tensile ductility remains unaffected at strain rates ≤10^{-2} s^{-1} but slowly decreases as strain rate is lowered, especially in the temperature regime of ~500-700°C. To better assess this effect, literature-reported changes in creep properties after low-dose irradiation in Alloy 316 and Alloy 316 weld metals are summarized in Figure 16. While the data show some scatter, creep strength can decrease by up to ~ 30% after irradiation. Meanwhile, creep ductility is shown to either increase or decrease by up to 20% (in base metal) or 70% (in weld metal) after irradiation. These data will be used to determine the appropriate environmental degradation factor for creep life of both the non-power test reactor and the commercial power reactor vessels.

Based on these literature data, no additional testing for irradiation embrittlement of material properties is required for either the non-power test reactor or the commercial power reactor. Instead, existing data will be used to develop degradation factors. However, irradiation tests of Alloy 316H, its heat affected zone, and ER16-8-2 weld filler metal will be conducted to better quantify design margins at the relatively low irradiation damage levels of the non-power test reactor and the commercial power reactor vessels. Details of the testing program will be provided with the operating license application.

4.2.6.2 Irradiation-Affected Corrosion

Corrosion in KP-FHR could be affected by irradiation through irradiation-induced changes in the redox potential of Flibe, irradiation-induced changes in the corrosion resistance of stainless steel, or both. In water-based systems, both mechanisms (water radiolysis and defect production in stainless steel) are thought to lead to irradiation-accelerated corrosion (Reference 58). However, these mechanisms are not applicable to the KP-FHR environment. First, Flibe is highly resistant to radiolysis because of the rapid recombination of ions in the molten state. Second, while irradiation could affect the chemistry of Flibe through transmutation, the chemistry control system will have the capability to adjust the redox potential of the salt and correct changes induced by transmutations, expected to be very small. Third, irradiation-induced defect in stainless steel can lead to radiation-enhanced diffusion, which may affect corrosion, but because of the high operating temperature of 550°C and the dpa rate of 0.1 dpa / [[

]]

the vacancy concentration is not significantly affected by irradiation, and radiation-enhanced diffusion is expected to be minimal.

Existing data indicates that irradiation effects are limited and can be both negative and positive. For example, Lei et al., show a modest increase in post-irradiation bulk corrosion rates (~3X faster) in FLiNaK salt after ~6.18 dpa irradiation with helium ions (Reference 59). In contrast, recent work by Short et al., indicates that simultaneous irradiation and corrosion in FLiNaK acts to minimize intergranular corrosion in molten salt (Reference 60 and 61). Apparently, increased near-surface vacancy concentrations from irradiation accelerates general corrosion (likely controlled via bulk diffusion) but increased intragranular vacancies promotes diffusion from grain interiors to the grain boundary, effectively lowering grain boundary corrosion rates.

Given that: (1) the only safety-related component that is subject to irradiation is the thick-walled reactor vessel, (2) the irradiation dose is quite low <0.1 dpa and (3) irradiation has shown a benefit to grain boundary corrosion (which is the primary concern), no immediate testing is planned. Instead, irradiation affected corrosion will be assessed via (1) a materials surveillance system program for the non-power test reactor and (at least the first) commercial power reactor systems and (2) an inspection and monitoring program that will assess the wall thickness of the reactor vessel. The initial plans for these programs are provided in Appendix B. Additional details of these plans will be provided in the operating license application.

4.2.6.3 Irradiation-Assisted Stress Corrosion Cracking (IASCC)

Similar to irradiation affected corrosion, IASCC is not an expected degradation mode in the KP-FHR. The two main pathways for IASCC in water environments are radiation effects on the water chemistry and on the materials (Reference 65). In the KP-FHR environment:

- Radiolysis of Flibe is not a concern, as detailed in in Section 4.2.6.2, and no irradiation-induced changes in the corrosion potential is expected;

- The accumulated dpa in the reactor vessel of <0.1 dpa, which is lower than the lower bound of ~3 dpa for IASCC observed in pressurized water reactors (Reference 65).

Furthermore, without significant hardening in the alloys at 0.1 dpa (Reference 51), and a potential benefit to grain boundary corrosion rates (Reference 60 and 61), there is no known mechanism by which irradiation would increase susceptibility to IASCC. The testing program will assess if stress corrosion cracking can occur in unirradiated materials (Section 4.2.4). However, available evidence indicates that this is not a credible degradation mechanism under conditions relevant to the KP-FHR. Since this test program is expected to show that there is no direct concern for stress corrosion cracking and since there is no clear means by which irradiation could increase susceptibility (i.e., no expected effect on the coolant chemistry, only a small amount of hardening at 0.1 dpa), no direct IASCC testing is planned at this time. Instead, this potential concern will be addressed via both surveillance samples and an inspection and monitoring program as discussed in Appendix B.

5 CONCLUSIONS AND LIMITATIONS

5.1 CONCLUSIONS

Alloy 316H base metal and ER16-8-2 weld filler metal have been selected as the metallic structural alloys for use in safety-significant, high temperature, Flibe-wetted component designs. This testing is being conducted to support the design and licensing of both the non-power test reactor (Hermes) and the commercial power generation reactor (KP-X). This testing is focused on structural alloys 316H and ER16-8-2 for the reactor vessel, which was determined to be the primary safety-related component of interest, as it serves to retain the Flibe coolant (a fission product barrier) around the fuel pebbles.

The materials testing consists of two major efforts: (1) testing in high temperature air to support ASME design (submitted for information) and (2) testing in molten Flibe salt to account for potential environmental degradation (submitted for review and approval). Testing to support design includes work to extend the code qualification of ER16-8-2 weld metal up to 816°C to match the current qualification of Alloy 316H base metal as well as testing and analyses required to support elastic-plastic and inelastic design per the ASME Code Section III, Division 5.

The environmental effects testing plan detailed in this report is based on an independent Expert Panel PIRT review for the operation of the commercial power generating reactor (KP-X). As detailed herein, the scope of testing for the non-power test reactor is reduced, based on the lower power and shorter time of operation relative to the commercial power reactor. While not required in the KP-FHR design for structural performance considerations, [[

]] . Appendix A of this report details cladding and coating materials that could be used with safety-related high temperature components of the KP-FHR. Such coatings do not affect structural performance of the underlying base metals and will be used consistent with ASME Section III code requirements.

Kairos Power is requesting Nuclear Regulatory Commission review and approval of the environmental effects testing plan described in this report for metallic structural materials used in safety-related Flibe-wetted areas high temperature components of the reactors for use by licensing applicants under 10 CFR 50 or 10 CFR 52. This includes approval of the planned testing and analyses to address potential materials reliability and environmental compatibility issues via design, operation, and inspection. The reactor vessel is credited for maintaining its integrity and retaining fluid to keep the fuel covered in salt during all normal operations and postulated events. The qualification plan for these materials support conformance, in part, to PDC 14 and PDC 31. The qualification plan intends to qualify the reactor vessel and safety-related Flibe-wetted areas and to maintain its integrity under the expected environmental conditions of the KP-FHR. The results of the planned tests and analyses, along with a description of the design and inspection program will be provided in a future license application.

5.2 LIMITATIONS

This report is limited to the qualification of metallic structural materials (Alloy 316H and ER16-8-2) for safety-significant, high temperature components in Flibe-wetted areas of the KP-FHR reactors.

6 REFERENCES

1. United States Nuclear Regulatory Commission, Regulatory Guide 1.203, *Transient and Accident Analysis Methods*, December 2005. (ML053500170).

2. Barua, B., et al. (2020). *Acceptance Criteria for the Mechanical Integrity of Clad/Base Metal Interface for High Temperature Nuclear Reactor Cladded Components*. Pressure Vessels & Piping. Minneapolis, MN USA, ASME: 1-8.

3. University of California Berkeley Nuclear Engineering. *Fluoride Salt Cooled High Temperature Reactor.* 2015.. [ONLINE] Available at:http://fhr.nuc.berkeley.edu. [Accessed 25 June 2020].

4. Kairos Power, LLC, *Design Overview of the Kairos Power Fluoride Salt Cooled, High Temperature Reactor,* KP-TR-001-P, Revision 1. February 2020. (ML20045E423).

5. Anderson, T.L., *Fracture Mechanics: Fundamentals and Applications*. 4th ed. 2017: CRC Press. 661.

6. Kairos Power, LLC, *Reactor Coolant for the Kairos Power Fluoride Salt-Cooled High Temperature Reactor,* KP-TR-004-P-A, Revision 1. July 31, 2020. (ML20219A591).

7. Kairos Power, LLC, *Principal Design Criteria for the Kairos Power Fluoride Salt Cooled High Temperature Reactor*, KP-TR-003-NP-A. June 2020. (ML20167A174).

8. Koger, J.W., *Evaluation of Hastelloy N Alloys After Nine Years Exposure to Both a Molten Fluoride Salt and Air at Temperatures from 700 to 560°C*. 1972, Oak Ridge National Laboratory. p. 1-44.

9. McCoy, H. E. and B. McNabb, *PostIrradiation Examination of Materials from the MSRE*, 1972, Oak Ridge National Laboratory. p. 1-104.

10. DeVan, J.H. and R.B. Evans, *Corrosion Behavior of Reactor Materials in Fluoride Salt Mixtures*. 1962, Oak Ridge National Laboratory.

11. Delpech, S., et al., *Molten Fluorides for Nuclear Applications.* Materials Today, 2010. 13(12): p. 34-42.

12. Walters, L., et al., *Sodium Fast Reactor Fuels and Materials: Research Needs*. 2011, Sandia National Laboratory. p. 1-74.

13. Mathew, M.D., R. Sandhya, and K. Laha, *Development of Structural and Steam Generator Materials for Sodium Cooled Fast Reactors.* Energy Procedia, 2011. 7: p. 250-256.

14. Courouau, J.-L., et al., *Corrosion by Liquid Sodium of Materials for Sodium Fast Reactors: the CORRONa Testing Device*, in *ICAPP*. 2011: Nice, France. p. 1-11.

15. Keiser, J.R., *Status of Tellurium-Hastelloy N Studies in Molten Fluoride Salts*. 1977, Oak Ridge National Laboratory. p. 1-31.

16. Keiser, J.R., J.H. DeVan, and E.J. Lawrence, *Compatibility of Molten Salts with Type 316 Stainless Steel and Lithium.* Journal of Nuclear Materials, 1979. 85&86: p. 295-298.

17. Koger, J.W., *Alloy Compatibility with LiF-BeF_2 Salts Containing ThF_4 and UF_4*. 1972, Oak Ridge National Laboratory. p. 1-52.

18. Zheng, G., et al., *Corrosion of 316 Stainless Steel in High Temperature Molten Li_2BeF_4 (FLiBe) Salt.* Journal of Nuclear Materials, 2015. 461: p. 143-150.

19. McCoy, H. E. and B. McNabb (1972), *Intergranular Cracking of INOR-8 in the MSRE*, Oak Ridge National Laboratory: 1-185.

20. McCoy, H.E., *Status of Materials Development for Molten Salt Reactors*. 1978, Oak Ridge National Laboratory. p. 1-38.

21. Ignatiev, V. and A. Surenkov, *Alloys Compatibility in Molten Fluorides: Kurchatov Institute Related Experience.* Journal of Nuclear Materials, 2013. 441: p. 592-603.

22. Ignatiev, V., et al., *Intergranular Tellurium Cracking of Nickel-Based Alloys in Molten Li, Be, Th, U/F Salt Mixture.* Journal of Nuclear Materials, 2013. 440: p. 243-249.

23. Cheng, H., et al., *Effects of Te on Intergranular Embrittlement of a Ni-16Mo-7Cr Alloy.* Journal of Nuclear Materials, 2015. 461: p. 122-128.

24. Cheng, H., et al., *EPMA and TEM Characterization of Intergranular Tellurium Corrosion of Ni-16Mo-7Cr-4Fe Superalloy.* Corrosion Science, 2015. 97: p. 1-6.

25. McNeese, L.E., *Molten-Salt Reactor Program Semiannual Progress Report*. 1976, Oak Ridge National Laboratory. p. 1-183.

26. vanRooyen, I.J., et al., *Advanced Electron Microscopy and Micro-Analytical Technique Development and Application on Irradiated TRISO-Coating Particles from the AGR-1 Experiment*. 2017, Idaho National Laboratory.

27. *High-Temperature Characteristics of Stainless Steels*, N.D. Institute, Editor., American Iron and Steel Institute: A Designer's Handbook Series. p. 1-44.

28. *The Role of Stainless Steel in Petroleum Refining,* in https://www.calbrite.com/industry-resources/, Iron and Steel Institute, Editor.1977. p. 1-57.

29. *Material Fabrication and Repair Considerations for Austenitic Alloys Subject to Embrittlement and Cracking in High Temperature 565-760^{o}C (1050-1400^{o}F) Refinery Services*. 2012, American Petrochemical Institute. p. 1-63.

30. Williamson, M., *Pyroprocessing Technologies: Recycling Used Nuclear Fuel for a Sustainable Energy Future*. 2019: Argonne National Laboratory.

31. Choi, E.-Y. and S.M. Jeong, *Electrochemical Processing of Spent Nuclear Fuels: An Overview of Reduction in Pyroprocessing Technology.* Progress in Natural Science: Materials International, 2015. 25: p. 572-582.

32. Simpson, M.F., *Developments of Spent Nuclear Fuel Pyroprocessing Technology at Idaho National Laboratory*. 2012, Idaho National Laboratory. p. 1-23.

33. Sim, J.-H., Y.-S. Kim, and I.-J. Cho, *Corrosion Behavior Induced by LiCl-KCl in Type 304 and 316 Stainless Steel and Copper at Low Temperature* Nuclear Engineering and Technology, 2017. 49: p. 769-775.

34. Kondo, M., et al., *Metallurgical Study on Corrosion of Austenitic Steels in Molten LiF-BeF_2 (Flibe).* Journal of Nuclear Materials, 2009. 386-388: p. 685-688.

35. NOT USED.

36. NOT USED.

37. ASME, *Boiler and Pressure Vessel Code*, in *High Temperature Reactors*. 2017, American Society of Mechanical Engineers.

38. International, A., *Standard Test Method for Creep-Fatigue Crack Growth Testing*. 2016, ASTM International. p. 1-19.

39. International, A., *Standard Test Methods for Conducting Creep, Creep-Rupture, and Stress-Rupture Tests of Metallic Materials*. 2018. p. 1-14.

40. ASME, *Development of Weld Strength Reduction Factors and Weld Joint Influence Factors for Service in the Creep Regime and Application to ASME Codes*. 2017, ASME. p. 1-376.

41. Spindler, M., *How to Prevent the Initiation of Cracks in Elevated Temperature Plant - The Gap between Design and Life Assessment*, R. McReynolds, Editor. 2019, EDF Energy. p. 1-34.

42. Young, G.A., M.J. Hackett, and T.-L. Sham, *Materials Challenges for Molten Salt Reactors*, in *1st International Conference on Generation IV and Small Reactors*. 2018, CNS: Ottawa, CA. p. 1-17.

43. Henthorne, M., *The Slow Strain Rate Stress Corrosion Cracking Test - A 50 Year Retrospective.* Corrosion. 72(12): p. 1488-1518.

44. International, A., *Standard Practice for Slow Strain Rate Testing to Evaluate the Susceptibility of Metallic Materials to Environmentally Assisted Cracking*, in *G129-00*. 2000, ASTM.

45. Jones, R.H. and R.E. Ricker, *Mechanisms of Stress-Corrosion Cracking*, in *Stress-Corrosion Cracking*, R.H. Johnes, Editor. 1992, ASM International: Metals Park, OH. p. 1-40.

46. Spindler, M.W. and M.C. Smith, *The Effect of Multiaxial States of Stress on Creep Failure of Type 316H Under Displacement Control*, in *Pressure Vessels and Piping Division Conference*. 2009, ASME: Prague, Czech Republic. p. 1-7.

47. Spindler, M., *Materials Issues in Advanced Gas Cooled Reactors*, R. McReynolds, Editor. 2019: British Energy. p. 1-55.

48. Miller, P.D. and W.K. Boyd, *Corrosion of Beryllium*. 1967, Battelle Memorial Institute: Columbus, OH. p. 1-38.

49. Higgins, J., *Precipitation in the Iron-Beryllium System.* Acta Metallurgica, 1974. 22(2): p. 201-217.

50. Zweibaum, N., et al., *Phenominology, Methods, and Experimental Program for Fluoride-Salt-Cooled, High-Temperature Reactors (FHRs).* Progress in Nuclear Energy, 2014. 77: p. 390-405.

51. Nagae, Y., et al., *Irradiation Effect on Mechanical Properties in Structural Materials of Fast Breeder Reactor Plant.* Journal of Nuclear Materials, 2011. 414: p. 205-210.

52. Zinkle, S.J. and G.S. Was, *Materials Challenges in Nuclear Energy*. Acta Materialia, 2013. 61: p. 735-758.

53. Bernard, J. and G. Verzeletti, *Elastic-Plastic Fracture Toughness Characteristics of Irradiated 316H Stainless Steel*, in *Elastic-Plastic Fracture Test Methods: The User's Experience, ASTM STP 856*, E.T. Wessel and F.J. Loss, Editors. 1985, ASTM. p. 131-149.

54. DeVries, M.I. *J-Integral Toughness of Low Fluence Neutron-Irradiated Stainless Steel*. in *13th International Symposium on the Influence of Radiation on Material Properties*. 1987. ASTM.

55. DeVries, M., et al. *Effects of Neutron Irradiation and Fatigue on Ductility of Stainless Steel*. in *Effect of Radiation on Structural Materials*. 1979.

56. NOT USED.

57. NOT USED.

58. Raiman, S.S., D.M. Bartels, and G.S. Was, *Radiolysis Driven Changes to Oxide Stability During Irradiation-Corrosion of 316L Stainless Steel in High Temperature Water.* Journal of Nuclear Materials, 2017. 493: p. 40-52.

59. Lei, G., et al., *Irradiation Accelerated Fluoride Molten Salt Corrosion of Nickel-Based UNS N10003 Alloy Revealed by X-Ray Absorption Fine Structure.* Corrosion Science, 2020. 165: p. 1-5.

60. Zhou, W., et al., *A Simultaneous Corrosion/Irradiation Facility for Testing Molten Salt-Facing Materials.* Journal of Physics Research B, 2019. 440: p. 54-69.

61. Zhou, W.Y., et al., *Proton Irradiation-Decelerated Intergranula Corrosion of Ni-Cr Alloys in Molten Salt.* Proquest Open Access, 2019: p. 1-11.

62. Cabrillat, M.T., et al., *Intergranular Reheat Cracking in 304H Components. Experiments and Damage Evaluation*, in *SMiRT*. 2001: Washington, DC. p. 1-8.

63. Spindler, M.W., *The Multiaxial Creep Ductility of Austenitic Stainless Steels.* Fatigue and Fracture of Engineering Structures, 2004. **27**: p. 273-281.

64. Bradford, R., *Austenitic Reheat Cracking*. 2015. http://rickbradford.co.uk/T73S04Tutorials.html.

65. Was, G.S., *Fundamentals of Radiation Materials Science*. 2007, Berlin: Springer-Verlag.

66. Aktaa J., et al., *Effects of hold time and neutron irradiation on the low-cycle fatigue behaviour of type 316-CL and their consideration in a damage model*. 2002. Nucl Eng Des. 213(2–3):111–117. doi:10.1016/S0029-5493(01)00511-8.

67. Pfeil P., et al., *Effects of irradiation in austenitic steels and other high-temperature alloys. In: Flow and Fracture of Metals and Alloys in Nuclear Environments*. 1965. ASTM International.

68. Tavassoli A-A., et al., *Data Collection on the Effect of Irradiation on the Mechanical Properties of Austenitic Stainless Steels and Weld Metals*. 1996. Eff Radiat Mater 17th Int Symp.:995-995–15. doi:10.1520/stp16521s.

69. Ward AL., *Thermal and irradiation effects on the tensile and creep rupture properties of weld deposited type 316 stainless steel*. 1974. Nucl Technol. 24(2):201–215. doi:10.13182/NT74-A31475.

70. Messner, M.C., et al., *Finite Element Analysis of Compliant Cladding and Base Metal Systems*. 2018, Argonne National Laboratory.

71. Messner, M.C., et al., *The Mechanical Interaction of Clad and Base Metal for Molten Salt Reactor Structural Components*, in *ASME Pressure Vessels and Piping*. 2018.

72. Barua, B., et al., *Development of Design Method for High Temperature Nuclear Reactor Cladded Components*, in *Pressure Vessels & Piping*. 2020, ASME: Minneapolis, MN, USA. p. 1-8.

73. Barua, B., et al., *Selection Criteria for Clad Materials to Use with a 316H Base Material for High Temperature Nuclear Reactor Cladded Components*, in *Pressure Vessels & Piping*. 2020, ASME: Minneapolis, MN, USA. p. 1-9.

74. Thoma, R.E., *Chemical Aspects of MSRE Operation*. 1971.

75. Brust, F. and J. Kennedy, *VFT Virtual Fabrication Technology Modeling & Simulation*, EMC-SQ, Editor. 2022, EMC^2: Columbus, Ohio. P. 1-5.

76. Draemel, D.C., *Faculty Research Associate, UC Berkeley*, G.A. Young, Editor. 2019.

77. Parker, T.D., *Strength of Stainless Steels at Elevated Temperature*, in *Source Book on Materials for Elevated-Temperature Applications*, E.F. Bradley, Editor. 1979.

78. Dhooge, A., *Reheat Cracking - A Reivew of Recent Studies.* International Journal of Pressure Vessels and Piping, 1987.

79. Dhooge, A., *Survey on Reheat Cracking in Austenitic Stainless Steels and Ni Base Alloys.* Welding in the World, 1998.

80. Chabuad-Reytier, M., et al., *Mechanism of Stress Relief Cracking in Titanium Stabilized Austenitic Stainless Steel.* Journal of Nuclear Materials.

81. Soundararrajan, S. and T.H. Hamad, *Stress Relaxation Cracking of TP 347H SS Flange Weld Joints on Reactor Charge Heater Manifold in Propane De-Hydrogenation Unit.*

82. Yoon, K.B., J.M. Yu, and T.S. Nguyen, *Stress Relaxation Cracking in 304H Stainless Steel Weld of a Chemical Reactor Serviced at 560°C.* Engineering Failure Analysis, 2015.

83. Chen, B., et al. *Effect of Thermo-Mechanical History on Reheat Cracking in 316H Austenitic Stainless Steel Weldments*. in *Pressure Vessels and Piping*. 2010.

84. Cabrillat, M.T., et al., *Intergranular Reheat Cracking in 304H Components. Experiments and Damage Evaluation*, in *SMiRT*. 2001.

85. Chartrand, P., C. Robelin, and A. Geribi, *A Thermodynamic Model for the LiF-BeF2-CrF2-CrF3-FeF2-FeF3-MoF3-Mo-F4-NiF2 System*. 2020, Polytechnique Montreal.

86. Spindler, M., *How to Prevent the Initiation of Cracks in Elevated Temperature Plant - The Gap between Design and Life Assessment*, R. McReynolds, Editor. 2019, EDF Energy.

87. Adamson, G.M., R.S. Crouse, and W.D. Manly, *Interim Report on Corrosion by Alkalai-Metal Fluorides*. 1953, Oak Ridge National Laboratory. p. 1-45.

88. Spindler, M.A., *An Assessment of the Creep Rupture Properties of Type 308 Weld Metal and Type 304/308/304 Weldments Using the PD6605 Procedure.*

89. Spindler, M.A., *The Multiaxial Creep Ductility of Austenitic Stainless Steels.* Fatigue and Fracture of Engineering Structures, 2004.

90. Skelton, R.P., et al., *Factors Affecting Reheat Cracking in the HAZ of Austenitic Steel Weldments.* Pressure Vessels and Piping, 2003.

91. Zweibaum, N., et al., *Phenominology, Methods, and Experimental Program for Fluoride-Salt-Cooled, High-Temperature Reactors (FHRs).* Progress in Nuclear Energy, 2014.

92. Guo, S., et al., *Corrosion in the Molten Fluoride and Chloride Salts and Materials Development for Nuclear Applications.* Progress in Materials Science, 2018.

93. Kelleher, B., et al., *Observed Redox Potential Range of Li2BeF4 Using a Dynamic Reference Electrode.* Nuclear Technology, 2016.

94. Afonichkin, V.K., A.L. Bovet, and V.V. Ignatiev, *Dynamic Reference Electrode for Investigation of Fluoride Melts Containing Beryllium Difluoride.* Journal of Fluorine Chemistry, 2009.

95. Duran-Klie, G., D. Rodriques, and S. Delpech, *Dynamic Reference Electrode Development of Redox Potential Measurements in Fluoride Molten Salt at High Temperature.* Electrochemica Acta, 2016.

96. Carotti, F., et al., *Electrochemical Sensors for On-Line Redox Measurements in Fluoride Salt-Cooled High Temperature Reactors*, in *American Chemical Society Fall Meeting*. 2020: (Virtual).

97. Swindeman, R.W., *The Mechanical Properties of INOR-8*. 1961, Oak Ridge National Laboratory.

98. Shrestha, S., et al., *Creep Resistance and Materials Degradation of Candidate Ni-Mo-Cr Corrosion Resistance Alloy for Application in a Molten Salt Reactor*. TMS Annual Meeting. 2015.

99. Rosenthal, M.W., P.N. Haubenreich, and R.B. Briggs, *The Development Status of Molten-Salt Breeder Reactors*. 1972, Oak Ridge National Laboratory.

100. Skowronski, N., *Tellurium-Induced Corrosion of Structural Alloys for Nuclear Applications in Molten Salts*. Nuclear Science & Engineering. 2917, Massachusetts Institute of Technology: Cambridge, MA. P. 1-12.

101. Wu, B.H., et al., *On the Origin of Tellurium Corrosion Resistance of Hot-Rolled GH3535 Alloy*. Corrosion Science, 2020. 170: p. 1-12.

102. Jia, Y., et al., *Effect of Temperature on Diffusion Behavior of Te into Nickel*. Journal of Nuclear Materials, 2013. 441: p. 372-379.

103. Cheng, H., et al., *Intergranular Diffusion and Embrittalment of a NI-16Mo-7Cr Alloy in Te Vapor Environment*. Journal of Nuclear Materials, 2015. 467: p. 341-348.

104. Liu, W., et al., *First-Principles Study of Intergranular Embrittlement Induced by Te in the Ni S 5 Grain Boundary*. Computational Materials Science, 2014. 88: p. 22-27.

105. Liu, W., et al., *The Effect of Nb Additive on Te-Induced Stress Corrosion Cracking in Ni Alloy: A First-Principles Calculation*. Nuclear Science and Techniques, 2014. 25(050603): p. 1-5.

106. Young, G.A., et al., *An Atomistic Modeling Study of Alloying Element, Impurity Element, and Transumtation Products on the Cohesion of a Nickel (100) Twist Grain Boundary*. 11th International Conference on Environmental Degradation of Materials in Nuclear Power Systems – Water Reactors. 2003. P. 1-10.

107. Briggs, R.B., *Molten-Salt Reactor Program Semiannual Progress Report for Period Ending August 31, 1962*. 1962, Oak Ridge National Laboratory. P. 1-158.

108. Jia, Y., et al., *Effect of SO4-2 Ion Impurity on Stress Corossion Behavior of Ni-16Mo-7Cr Alloy in FLiNaK Salt*. Journal of Nuclear Materials, 2021. 547: p. 1-8.

109. Young, G.A., N. Lewis, and D.S. Morton, *The Stress Corrosion Crack Growth Rate of Alloy 600 Heat Affected Zones Exposed to High Purity Water*. Conference on Vessel Penetration Inspection, Crack Growth, and Repair. 2003, US NRC: Gathersburg, MD. P. 371-386.

110. Xu, J., et al., *Short-Term Creep Behavior of an Additive Manufactured Non-Weldable Nickel-Base Superalloy Evaluated by Slow Strain Rate Testing*. Acta Materialia, 2019. 179: p. 142-157.

111. Norman, V. and M. Calmunger, *An Accelerated Creep Assessment Method Based on Inelastic Strain Partitioning and Slow Strain Rate Testing*. Materials & Design, 2021. 205: p. 1-14.

112. Shahinian, P., H.H. Smith, and J.R. Hawthorn, *Fatigue Crack Propagation in Stainless Steel Weldments at High Temperature.* Welding Journal Research Supplement, 1972. 11: p. 527-533.

113. Shahinian, P., H.H. Smith, and H.E. Watson, *Fatigue Crack Growth in Type 316 Stainless Steel at High Temperature.* Transactions of the ASME, 1971: p. 976-980.

114. James, L.A., *Crack Propagation Behavior in Type 304 Stainless Steel Weldments at Elevated Temperature.* Welding Journal Research Supplement, 1973: p. 173-179.

115. Maeng, W.Y. and Y.H. Kang, *Creep-Fatigue and Fatigue Crack Growth Properties of 316LN Stainless Steel at High Temperature*, in *Transactions of the 15th International Conference on Structural Mechanics in Reactor Technology*. 1999: Seoul, Korea. p. 1-8.

116. Mehmanparasat, A., *The Influence of Inelastic Damage on Creep, Fatigue, and Fracture Toughness*, in *Mechanical Engineering*. 2012, Imperial College: London. p. 297.

117. Hasegawa, K. and S. Usami, *Effect of Stress Ratio on Fatigue Crack Growth Threshold for Austenitic Stainless Steels in Air Environment.* Key Engineering Materials, 2017. 741: p. 88-93.

Table 1. Summary of Key Parameters for the Power Reactor and the Non-Power Test Reactor

Parameter	Power Reactor	Non-Power Test Reactor
Reactor Description	Low pressure, fluoride salt-cooled high temperature reactor (FHR)	
Core Configuration	Pebble bed core, graphite reflector, and enriched Flibe molten salt coolant	
Physical Dimensions	Reactor Vessel is ~4 m diameter, ~6 m height	Reactor Vessel is ~2.5 m diameter, ~4 m height
Reactor Thermal Power	320 MW_{th}	35 MW_{th}
Primary Heat Transport System	Flibe Salt, 550°C-650˚C, ~0.2 MPa, ~0.11-0.15 m/s	
Intermediate Heat Transport System	Intermediate Coolant, <0.2 MPa, 360°C-600°C	None. Primary Heat Transport System rejects heat to the (air) heat rejection subsystem
Power Conversion System	300°C-585°C, steam ~19 MPa	None. Primary Heat Transport System rejects heat to the (air) heat rejection subsystem
Material for Safety-Related Structures	Alloy 316H and ER16-8-2 (ASME Section III, Division 5, approved)	
Lifetime	[[ ]]	≤5 years (1 year commissioning + 4 years operation)
End of Life Irradiation of Reactor Vessel	<0.1 dpa	

Table 2. Ranking of Structural Alloys for FHR Applications

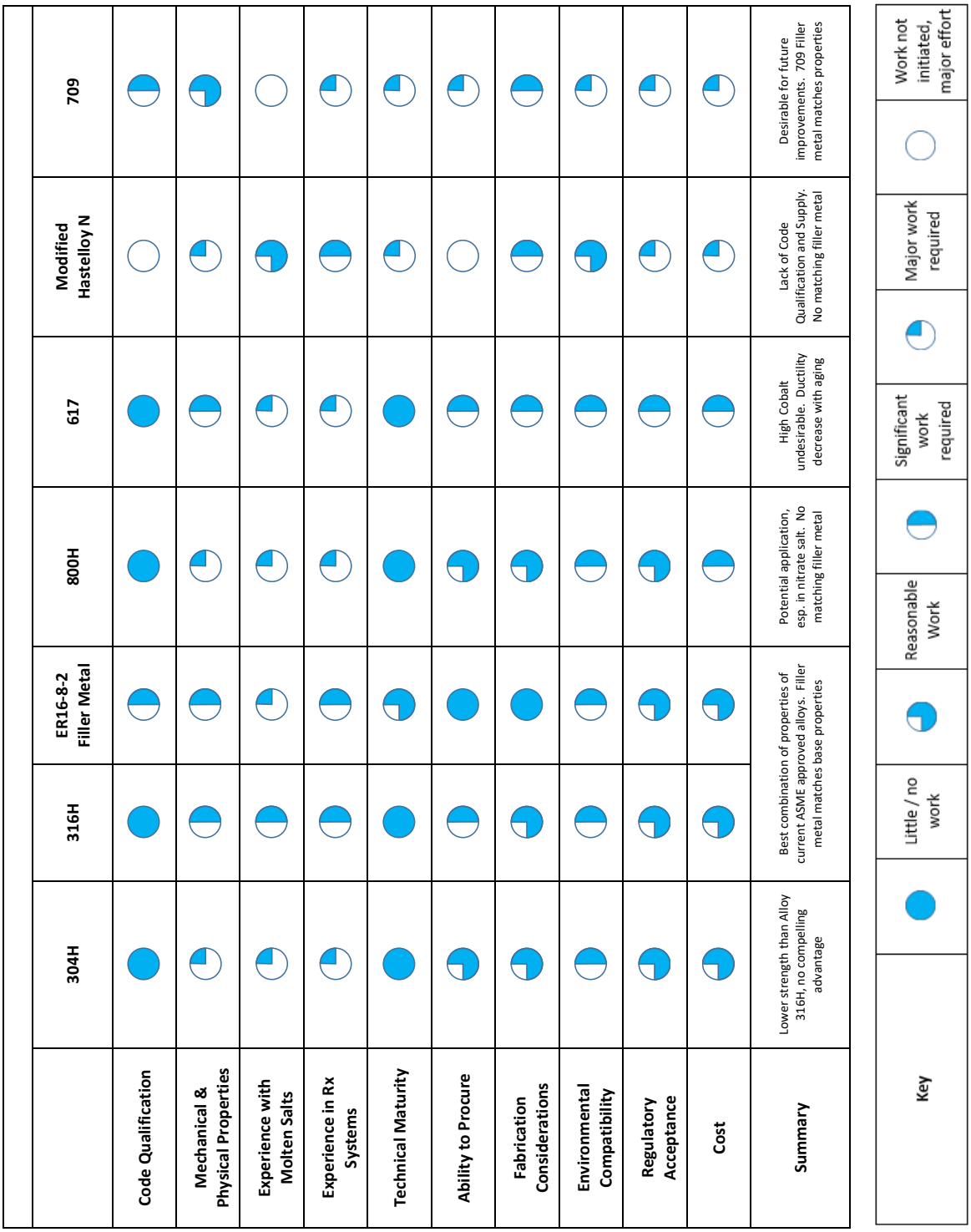

Table 3. Summary of Tests to Extend the ASME Qualification of ER16-8-2 to 816°C

[[

]]

Table 4. Summary of Tensile Tests to Support Non-Power Test Reactor Design

[[

]]

Table 5. Summary of Stress Relaxation Tests to Support Non-Power Test Reactor Design

[[

]]

Table 6. Summary of Strain Rate Change (aka 'stress dip') Tests to Support Non-Power Test Reactor Design

[[

]]

Table 7. Summary of Uniaxial Creep Tests to Support Non-Power Test Reactor Design

[[

]]

Table 8. Summary of Notched Bar Creep Tests to Support Non-Power Test Reactor Design

[[

]]

Table 9. Summary of Creep-Fatigue Tests to Support Non-Power Test Reactor Design

[[

]]

Table 10. Summary of Potential Testing to Assess Stress Relaxation Cracking

[[

]]

Table 11. Summary of Testing and Analysis Judged to be Warranted by the Materials PIRT Review

[[

]]

Table 12. Overall Effects that will be Assessed to Develop Corrosion Rate Models

[[

]]

Table 13. Detailed Plans for Corrosion Testing

[[

]]

Table 14. Summary of Slow Strain Rate Testing to Assess Environmentally Assisted Cracking

[[

]]

Table 15. Conditions for Corrosion Fatigue Crack Growth Rate and Stress Corrosion Cracking Tests

[[

]]

Table 16. Test Conditions to Assess Creep-Rupture Performance in Flibe

[[

]]

Table 17. Specimens for Characterization to Assess Metallurgical Effects

[[

]]

Table 18. NOT USED

Table 19. NOT USED

Table 20. Summary of Observations Intergranular Corrosion and EAC in Structural Alloys in Fluoride Salts or in Known Embrittling Contaminant

Alloys	Environment	Temp. (°C)	Time (hr)	Stress (MPa)	Notes	References
OFHC Cu	MSRE Fuel Salt ($LiF-BeF_2-UF_4$)	>500	13,000	Unknown. Plastically Deformed	Extensive IGSCC, unclear if corrosion-deposit (rich in Ni, Fe, Cr, Mo) influenced.	Reference 9
INOR-8	11.2NaF-41KF-45.3LiF-2.5UF4 (mol %)	593-982	≤1200	14-207	Creep tests. Cracking is intergranular in both air and molten salt. Salt exposure does not degrade creep life.	Reference 97
INOR-8	Air with intentional contamination of Te, Se, S, etc.	~650	~2000	Strained to failure	S, Se, Te cause intergranular cracking. Cracks are deeper if stressed material exposed to Te	Reference 99
Ni Alloys	$LiF-BeF_2-ThF_4$ 72-16-12 mol.%)	~645	Not specified	Not specified	Ni-S eutectic noted to lead to intergranular attack and failure of processing equipment	Reference 25
304 SS Hast. N, Hast. S, A600 Mod. Hast. N	Fuel salt (Flibe) contaminated with Cr_3Te_4 and Cr_5Te_6	700	2500	Post-exposure strain to failure at room T	Ni alloys are susceptible to Te induced IG cracking under oxidizing potentials. 304 SS & other Fe alloys resistant. ~1.5 wt.% Nb to Hast N imparts resistance, Ti+Nb negates effect.	Reference 20
Ni alloys near Hast N.	Fluoride Salts + Cr_3Te_4	750	400	80 MPa	Applied stress increases the number density and depth of intergranular cracks	Reference 21
Ni-16Mo-6.4Cr-3.6Fe	FLiNaK	700	~250	190 MPa (~75% YS, 40% of UTS) (creep)	Extensive intergranular cracking. Creep failure time ~ 50% that in air. Salt thought to accelerate creep failure by preferentially corroding Mo depleted grain boundaries	Reference 98
GH3535 (Ni-16Cr-6Cr)	Te Vapor	25	150 hrs at 800°C prior to room temperature test	Tensile test to failure	≤90 µm of intergranular cracking.	Reference 101
Hastelloy N	FLiNaK + 500 ppm SO_4^{-2}	700	400	C-ring, 25% UTS (elastic) and 75% UTS (plastic)	Increase corrosion relative to no SO_4^{-2} but no SCC. Stress increases depth of oxidized layer with sulfate but stress has little effect on Cr loss depth. S diffuses into grain boundaries and (Mn,Cr)S observed	Reference 108
316L/316	FLiNaK	600	≤125	1e-6 SSRT to failure	~1e-6 SSRT test to failure. Gauge shows extensive IG, shoulder less, grip none. Analysis indicates sulfur embrittlement under oxidizing conditions	This Work
316H	Flibe	600	≤125	1e-6 SSRT to failure	Limited grain boundary cracking observed. No association with sulfur. Tensile elongation [3] air testing.	

Table 21. Comparison of the Expected Reactor Vessel Irradiation Damage

Reactor System	Expected Vessel DPA at End of Life	Expected Helium in Reactor Vessel at End of Life
Non-Power Test Reactor	<0.1	<10 at. ppm
Commercial Power Reactor		<15 at. ppm

Figure 1. NOT USED

Figure 2. Overview of the Commercial Power Generation Reactor Heat Transport Loops with Nominal Operating Temperatures

[[

]]

Figure 3. Comparison of the Operating Pressures and Temperatures of Selected Conventional and Advanced Reactor Designs

[[

]]

Note: The labels refer to pressurized water reactors (PWR), boiling water reactors (BWR), high temperature gas reactors (HTGR), and sodium fast reactors (SFR)

Figure 4. Comparison of the Operating Conditions of Alloy 316H in the KP-FHR (blue box) with Oil & Gas Refinery Components and Existing Creep Rupture Data

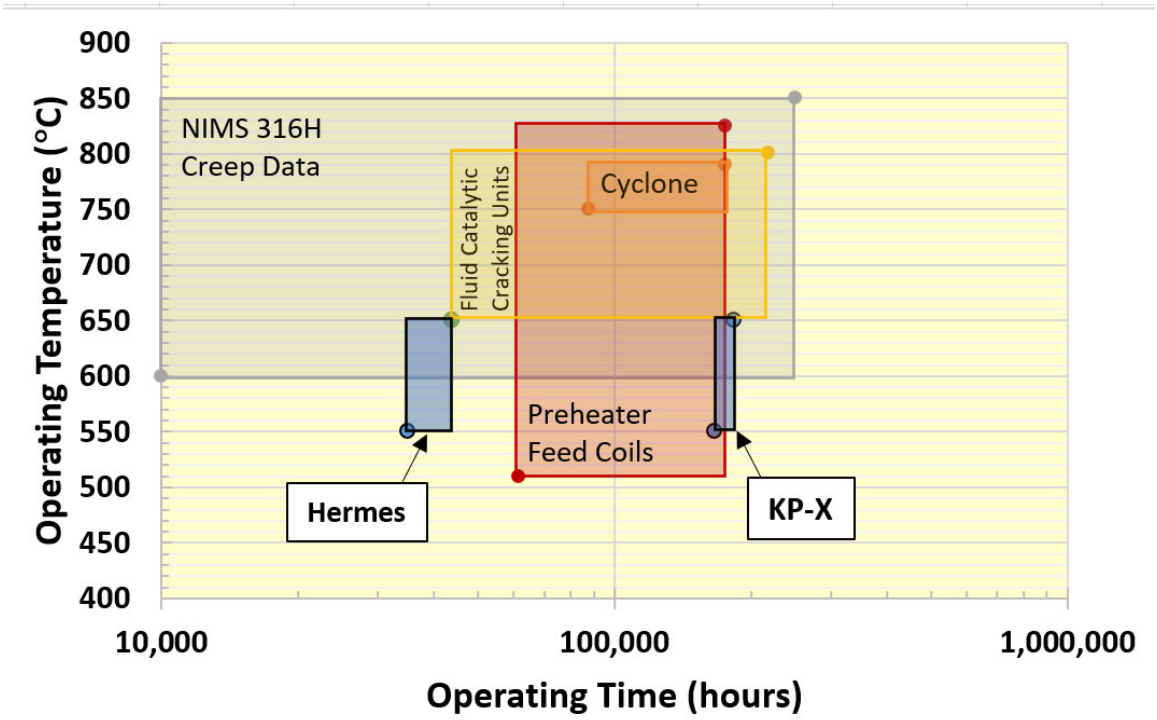

Note: Application of Alloy 316H and its weld metals in the KP-FHR is consistent with other industrial use

Figure 5. NOT USED

Figure 6. Illustration of the Environmental Degradation Mechanisms Considered in the Kairos Power PIRT Review of Environmental Degradation

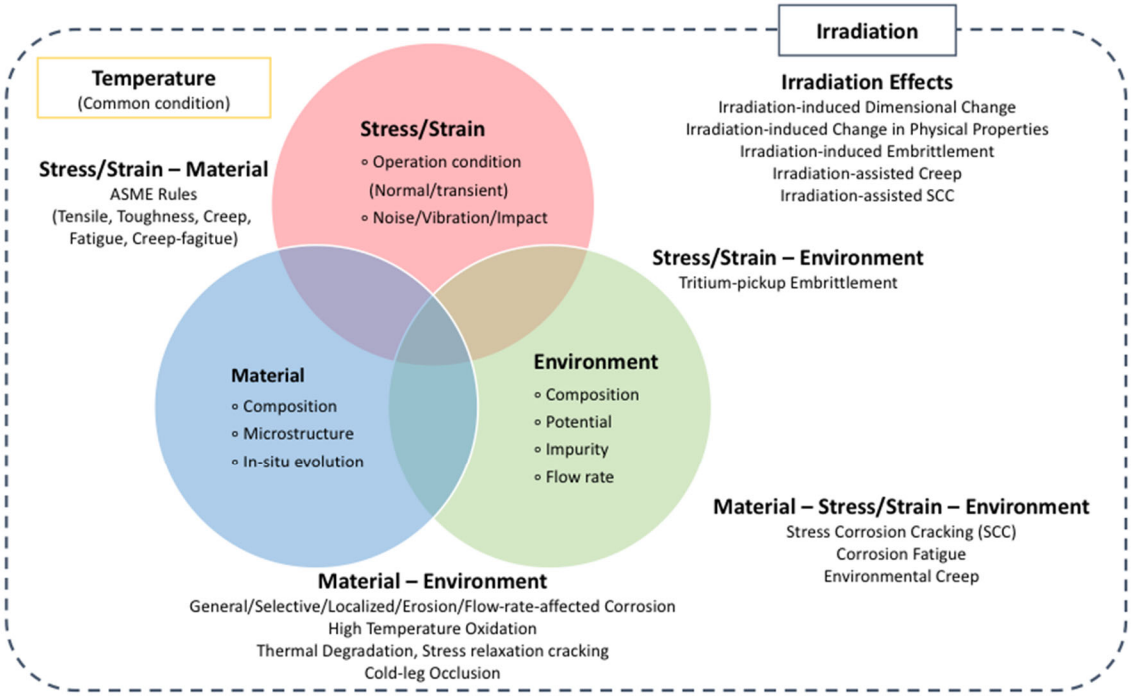

Figure 7. The Knowledge and Importance Rankings Used by the Expert Panel to Assess Environmental Degradation Phenomena

		Knowledge		
		High	*Medium*	*Low*
Importance	*High*	Category #4	Category #2	Category #1 (most important)
	Medium	Category #6	Category #5	Category #3
	Low	Category #9 (least important)	Category #8	Category #7

Figure 8. Summary of the PIRT Rankings

[[

]]

Figure 9. Illustration of the Combined Corrosion Monitoring Approach

[[

]]

Figure 10. Illustration of Slow Strain Rate Testing (SSRT) Data (left) and How the Results May Be Used to Map Out Regimes of Susceptibility to Environmentally Assisted Cracking (right)

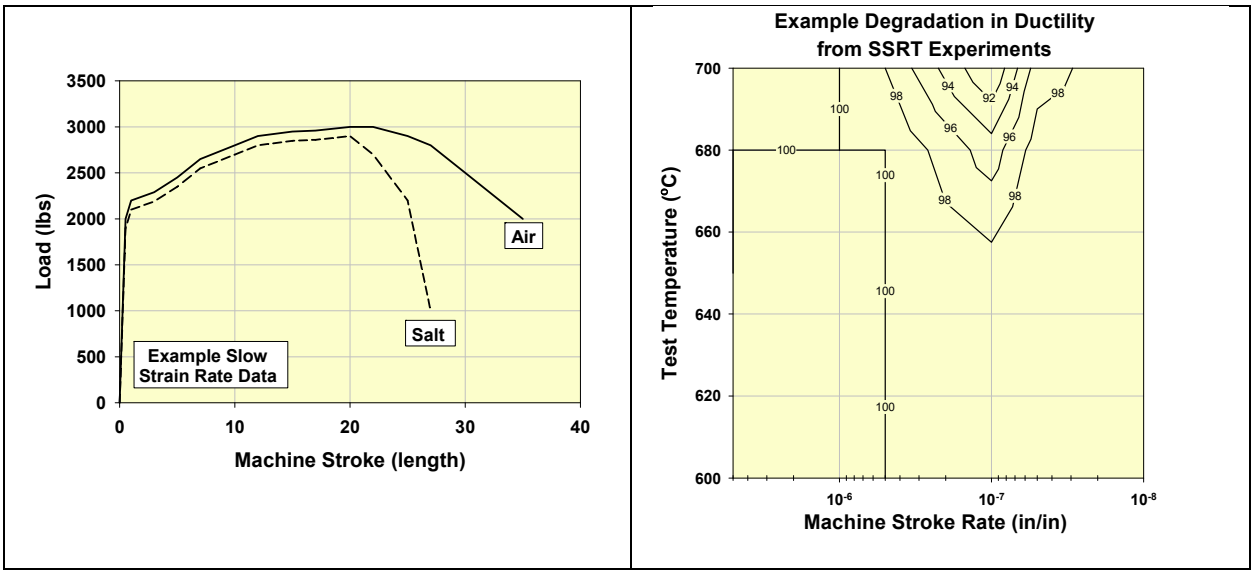

Figure 11. Example Corrosion Fatigue Crack Growth Rate Data (left) and How They Will be Compared to Data Collected in Air (right) to Assess the Effect of Environment

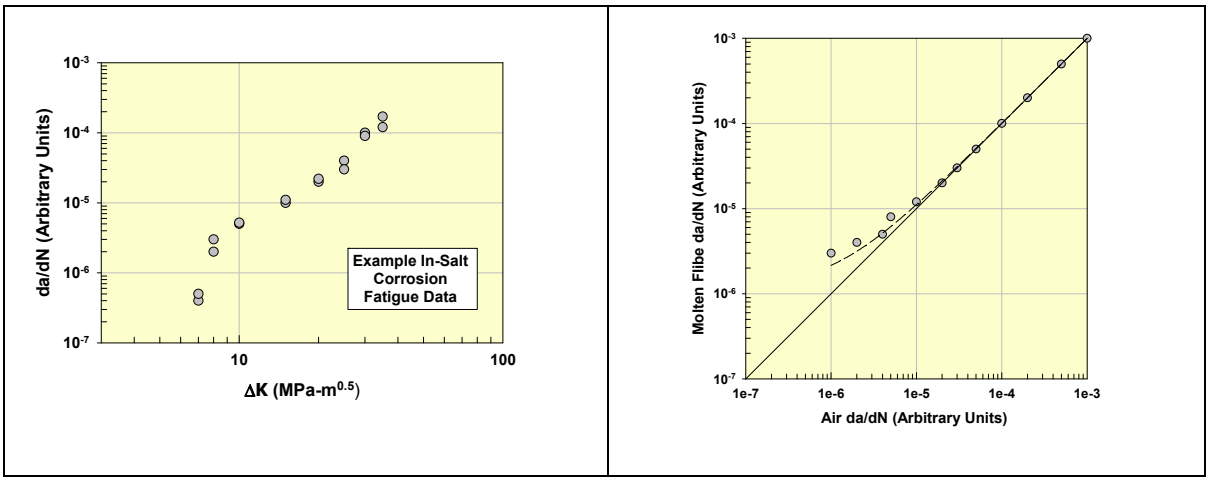

Figure 12. Illustration of a Potential SCC Mechanism in Flibe (top) where Grain Boundary Cr Loss is Accelerated at a Strained Crack Tip and (bottom) Schematic SCC Growth Rate Data

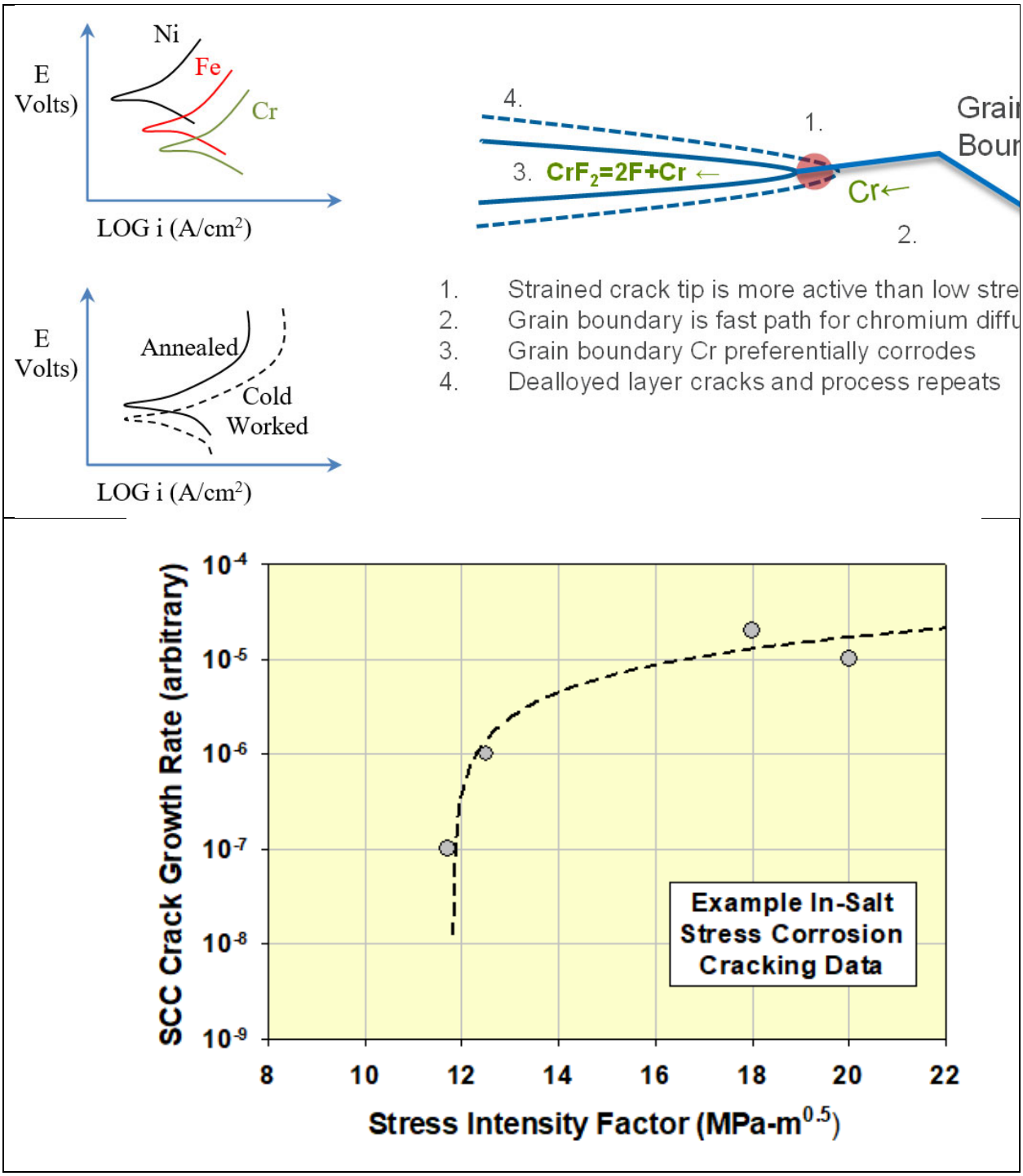

Figure 13. Illustration of Irradiation Dose and Helium Production Vary as a Function of Time in the Commercial Power Reactor Vessel

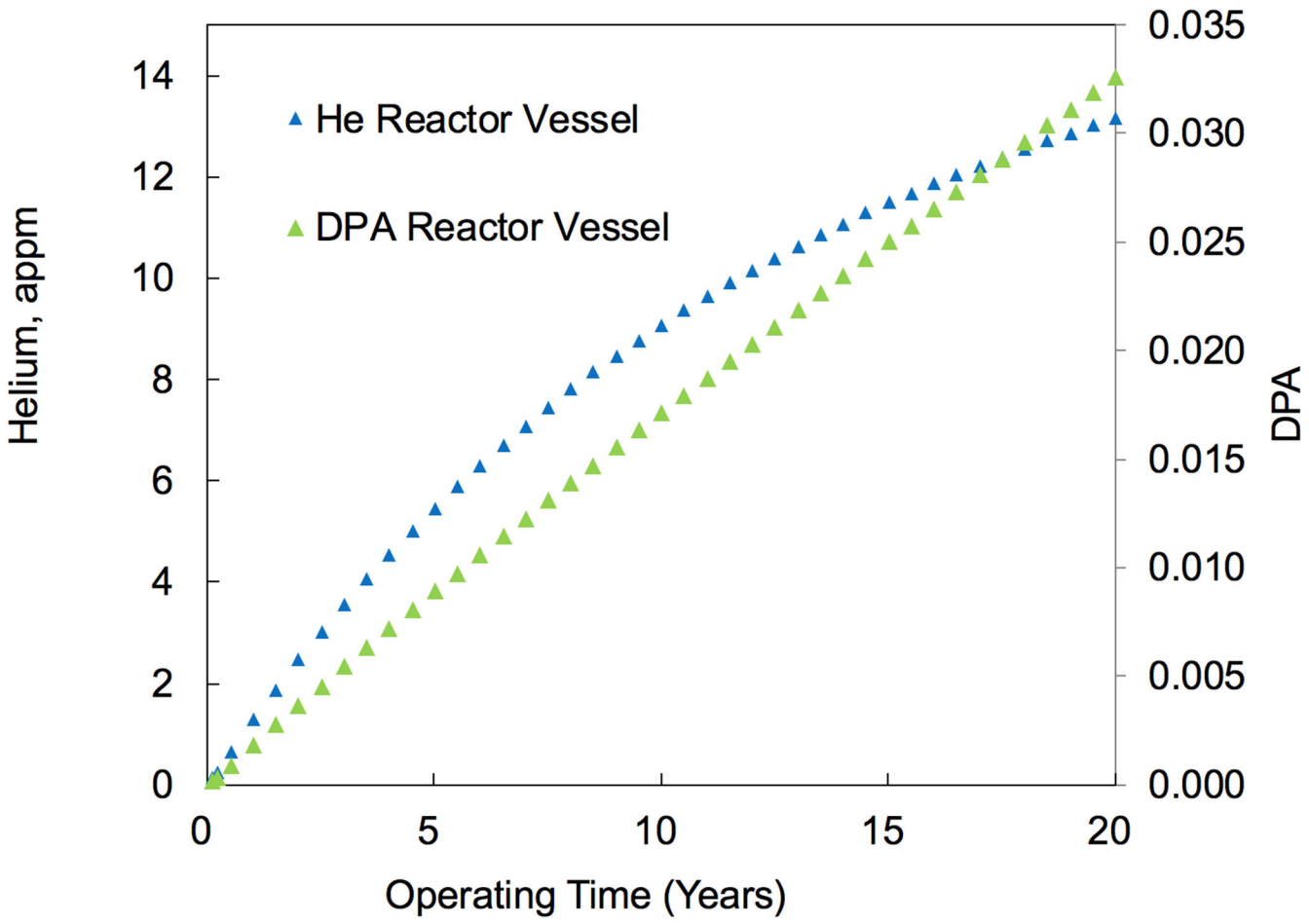

Figure 14. How Irradiation Affects Fracture Toughness in Austenitic Stainless Steels and Specific Data for Alloy 316 and 304 at 550°C.

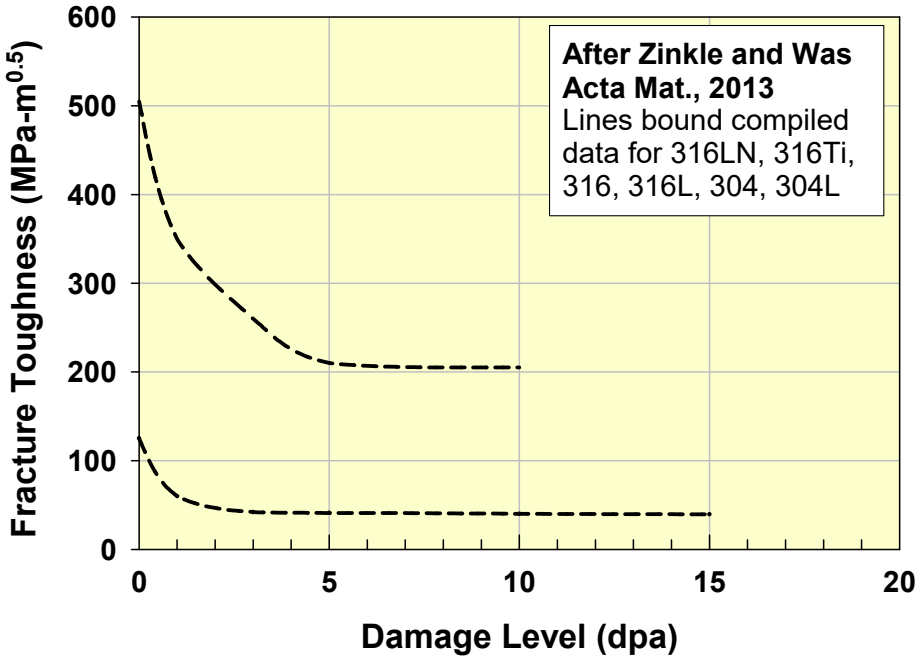

Note: Reference 52

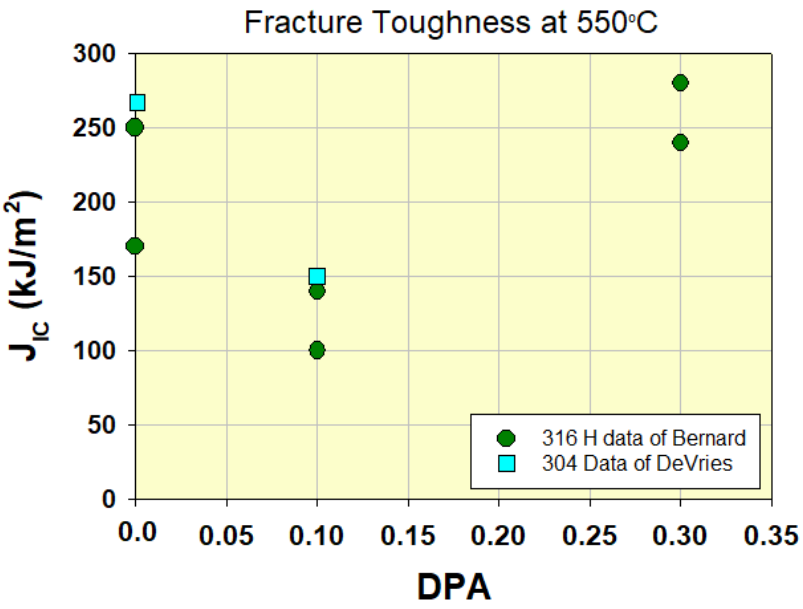

Note: Reference 53 and 54

Figure 15. Illustration of How Strain Rate and Temperature Affect Tensile Ductility in an Austenitic Stainless Steel Irradiated to a Helium Content of ~7 at. ppm

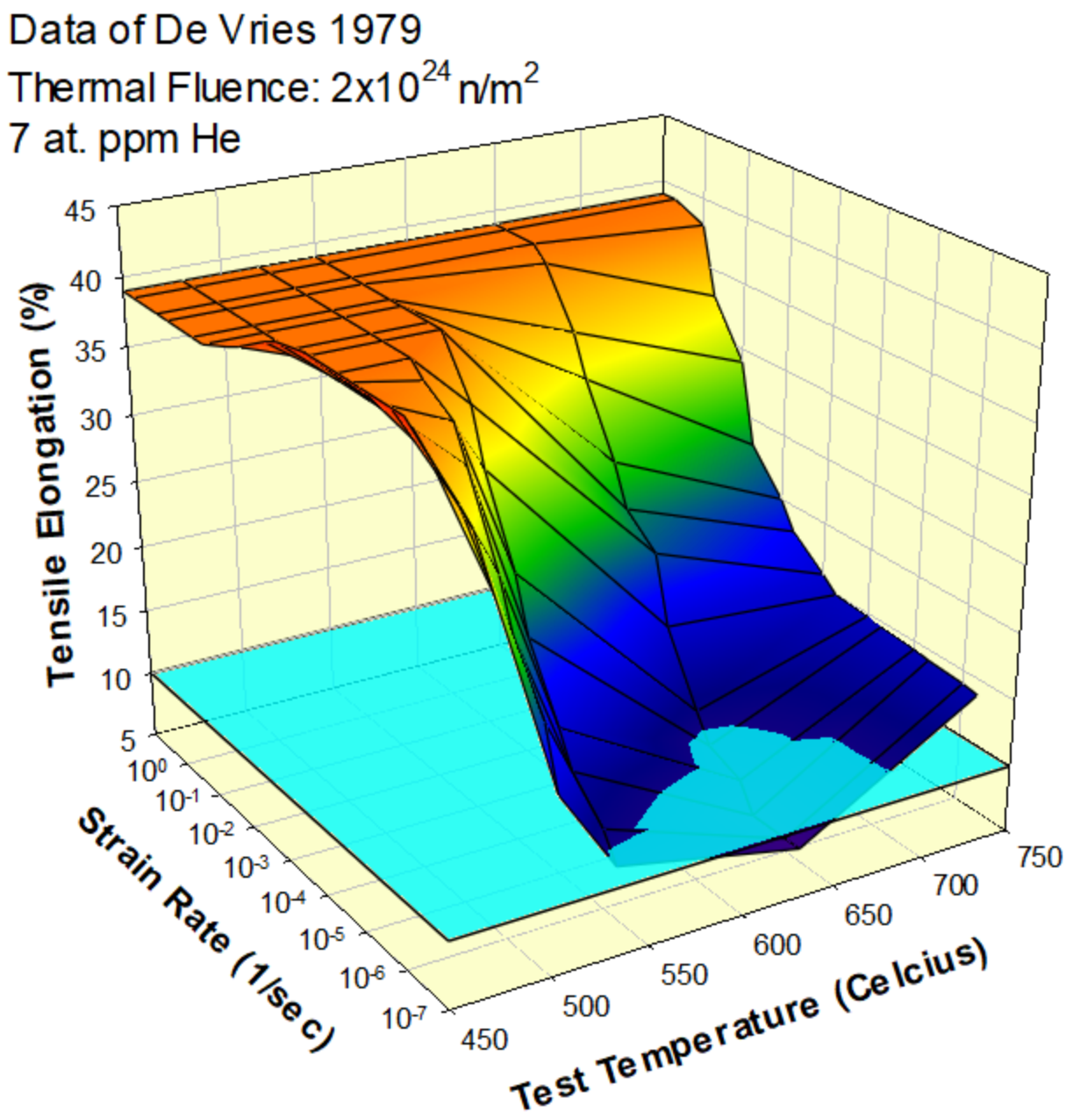

Note: Reference 55

Figure 16. (a) Normalized Creep Strength After Irradiation (Ratio of Irradiated Stress to Unirradiated stress to Reach the Same Average Creep Life) (b) Normalized Creep Ductility After Irradiation (Ratio of Irradiated Ductility to Unirradiated Ductility at the Same Stress

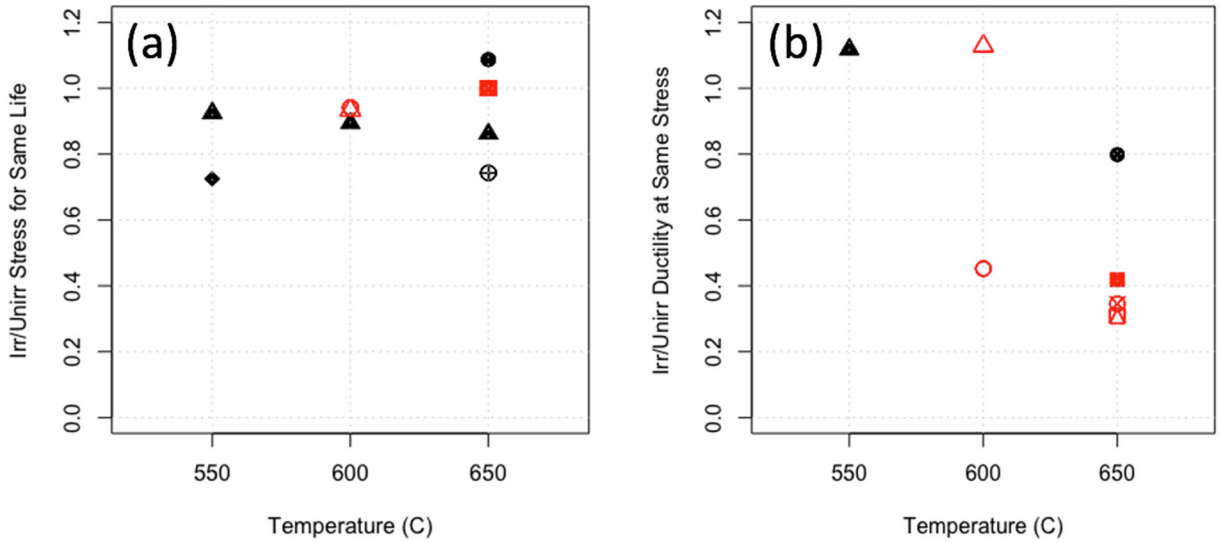

Note: References 56, 66, 67, 68, 69

Figure 17. Variable Corrosion Rate of Alloy 316 Stainless Steel with Time (top) and The Strong Benefit of Be Addition (Redox Control) (bottom).

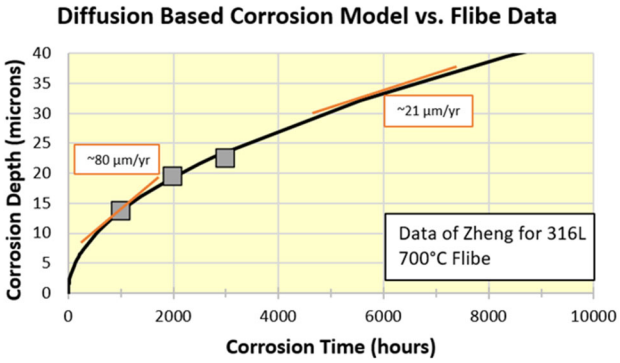

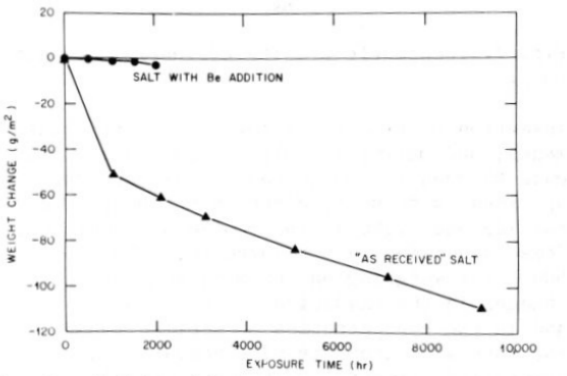

Fig. 2. Weight change versus exposure time for type 316 stainless steel in LiF-BeF_2 salt at the maximum loop temperature of 650°C.

Figure 18. Data of Zheng et al, Illustrating the Effect of Graphite on the Corrosion Depth (top) and Corrosion Rate of Alloy 316L in Flibe at 700°C (right)

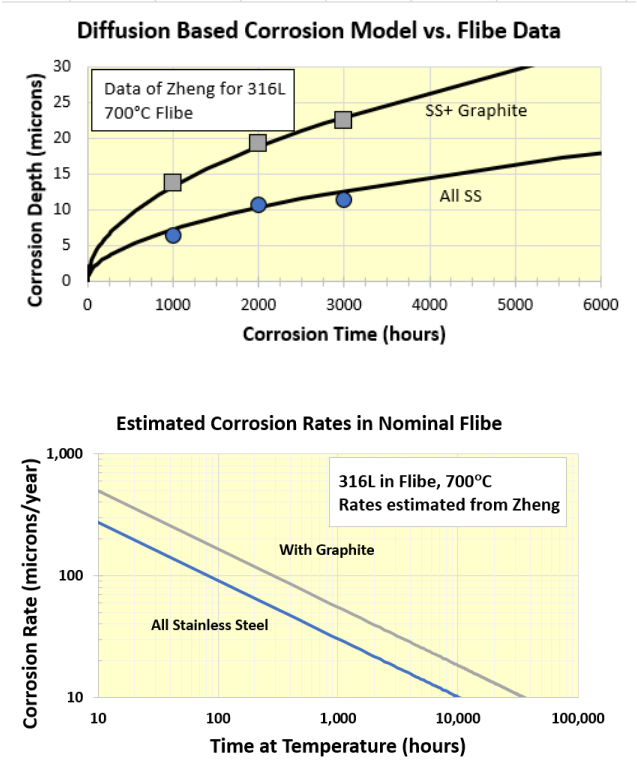

Note: The difference in corrosion rate is just less than 2X

Figure 19. Examples of Weld Pad Buildups (top) and A V-Groove Weld (bottom) used to Fabricate Test Samples

[[

]]

Figure 20. Comparison of the Composition of Heat 578409 (+ symbols) Relative to the ASME Code Specification (dashed lines, from Section II. 2017)

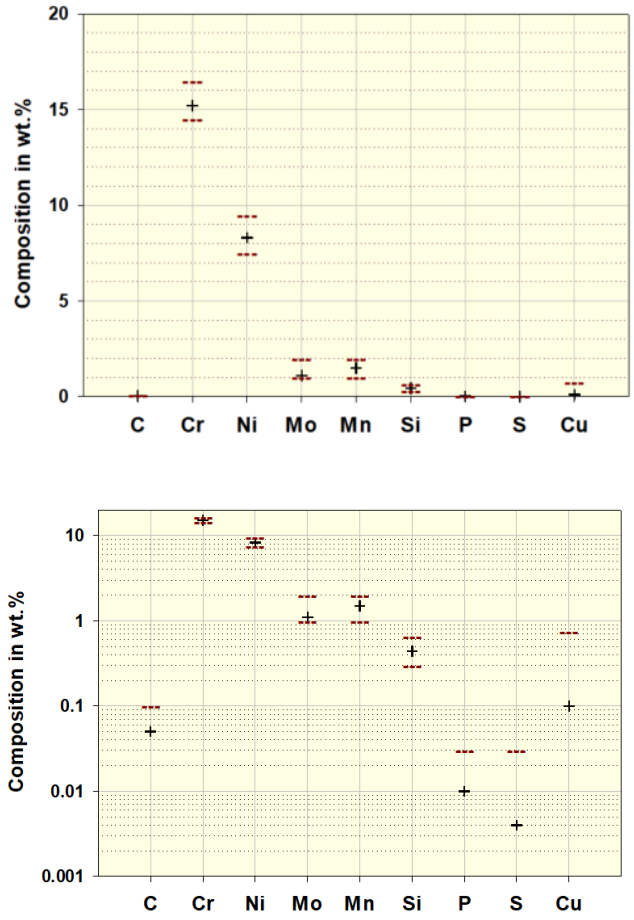

Note: C, P, S, and Cu only have maximum specifications. Linear scale (top) and log scale (bottom) to better illustrate the elements at low concentrations.

Figure 21. Selected Creep-Rupture Data for ER16-8-2 Weld Filler Metal Compared to the Best Estimate Prediction and Confidence Bounds

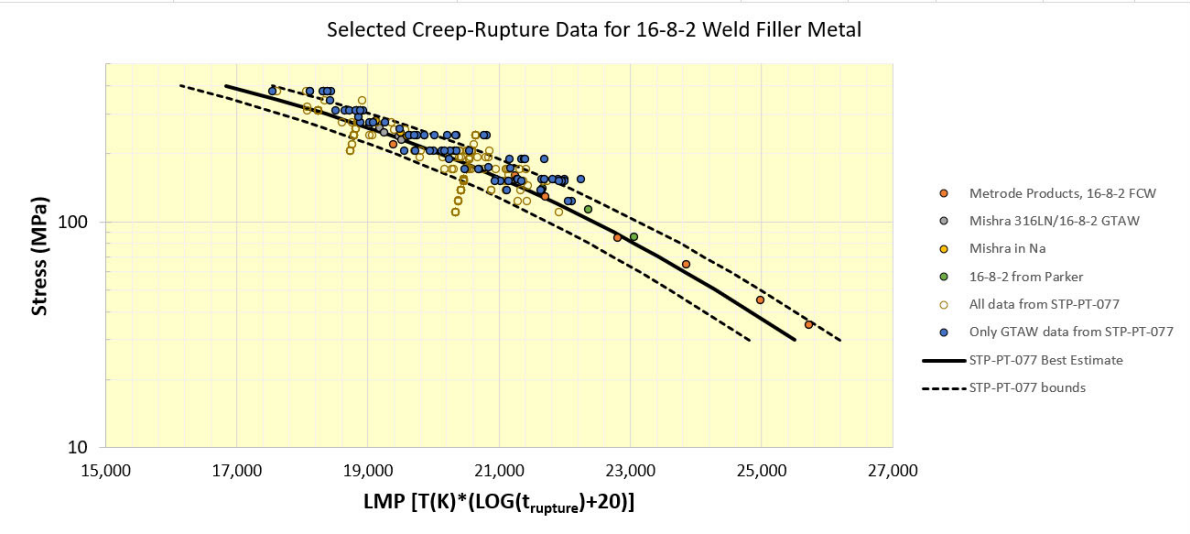

Note: Presented in STP-PT-077. The ASME Code Case data will be assessed relative to relevant data and appropriate statistical bounds determined.

Figure 22. Comparison of Selected Base Metal and Weld Metal Tensile Data

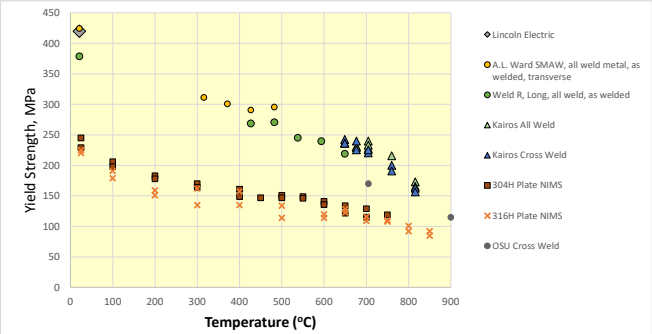

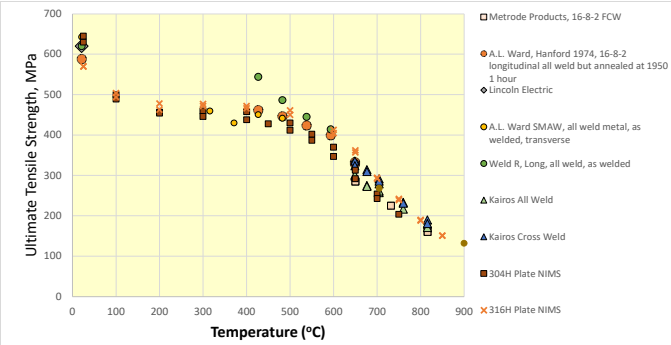

Note: Yield strength shown on the top and ultimate tensile strength on the bottom.

Figure 23. Weld Designs that Minimize the Risk of Stress Relaxation Cracking

[[

]]

Figure 24. Illustration of a Narrow Groove Gas-Tungsten-Arc Weld with the Location of a Notched Tensile Bar Overlayed in the Heat Affected Zone

[[

]]

Figure 25. Potential Location of the CCS Relative to the Reactor Vessel

[[

]]

Figure 26. Predicted Grain Boundary Diffusion Rate

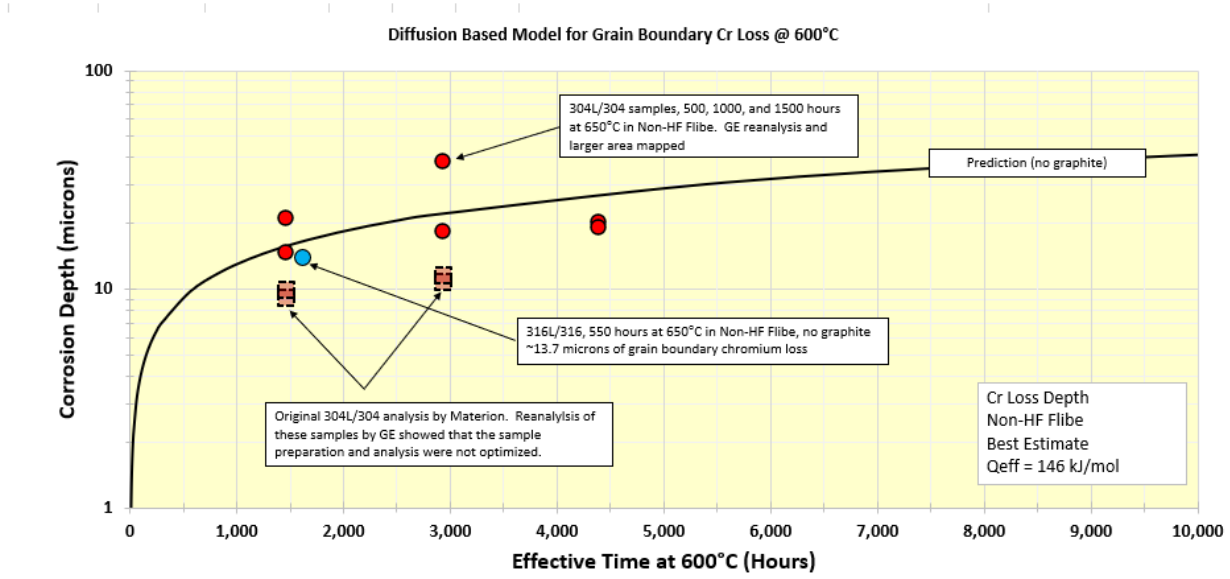

Note: Predicted grain boundary diffusion rate (solid black line) with recent data for Alloy 304 (red points) and Alloy 316 (blue point). For the Alloy 304L/304 data, two separate analyses are included but the red points (large area, GE analysis) are judged to be the most accurate. Based on the small surface area of graphite in the Alloy 304L/304 tests, comparison with the no graphite curve is appropriate.

Figure 27. Schematic Illustration of a Rotating Cage Loop (RCL) Corrosion Testing System (left) and an Operational RCL System (right)

[[

]]

Figure 28. Example of Fluoride Salt Compositional Analysis

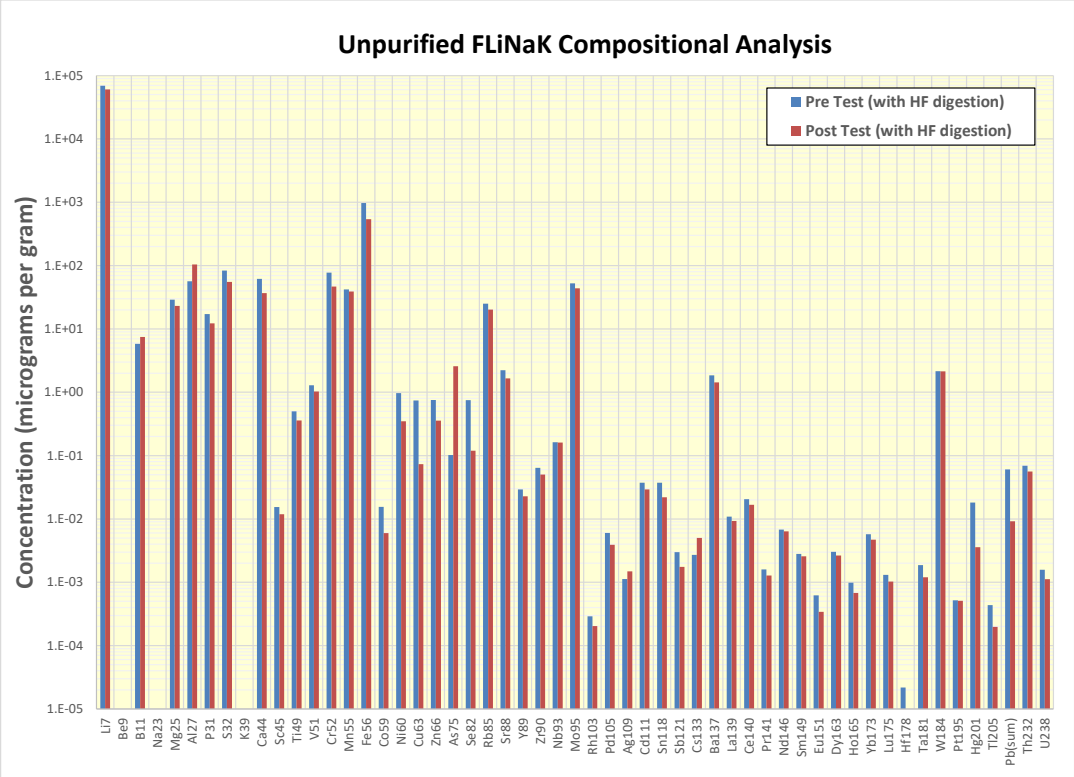

Note: Unpurified FLiNaK before and after SSRT testing an Alloy 316L sample at 600°C and 1e-6 (in/in)/sec

Figure 29. The Time-Temperature-Transformation Diagram for Alloy 316H

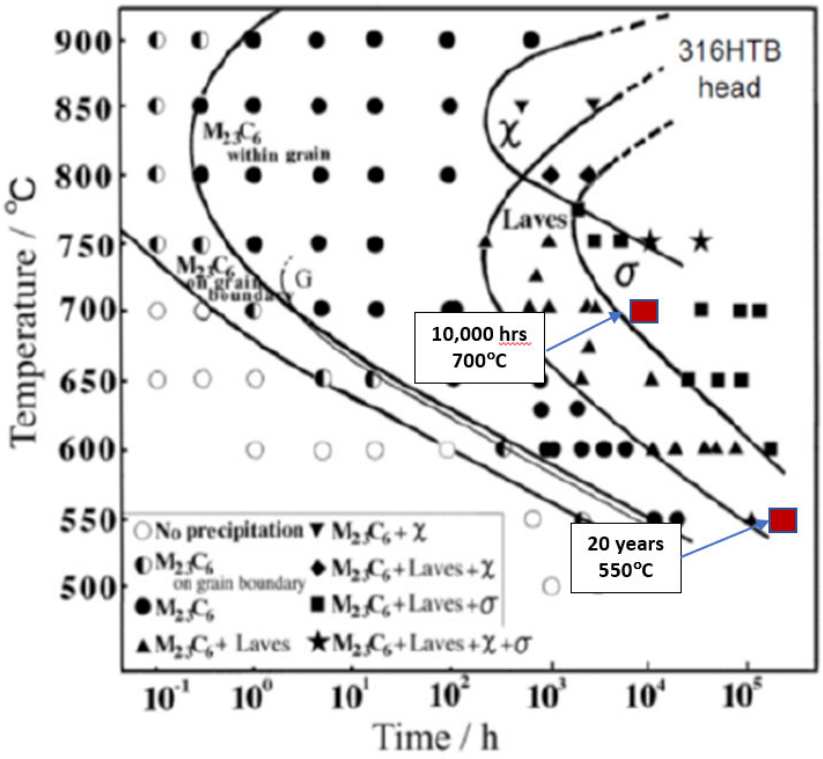

Note: Targeting 700°C for 10,000 hours as an aging treatment to represent long time operation at 550°C (Reference 82)

Figure 30. Calculated LiF-BeF_2 Phase Diagram Against Experimental Data

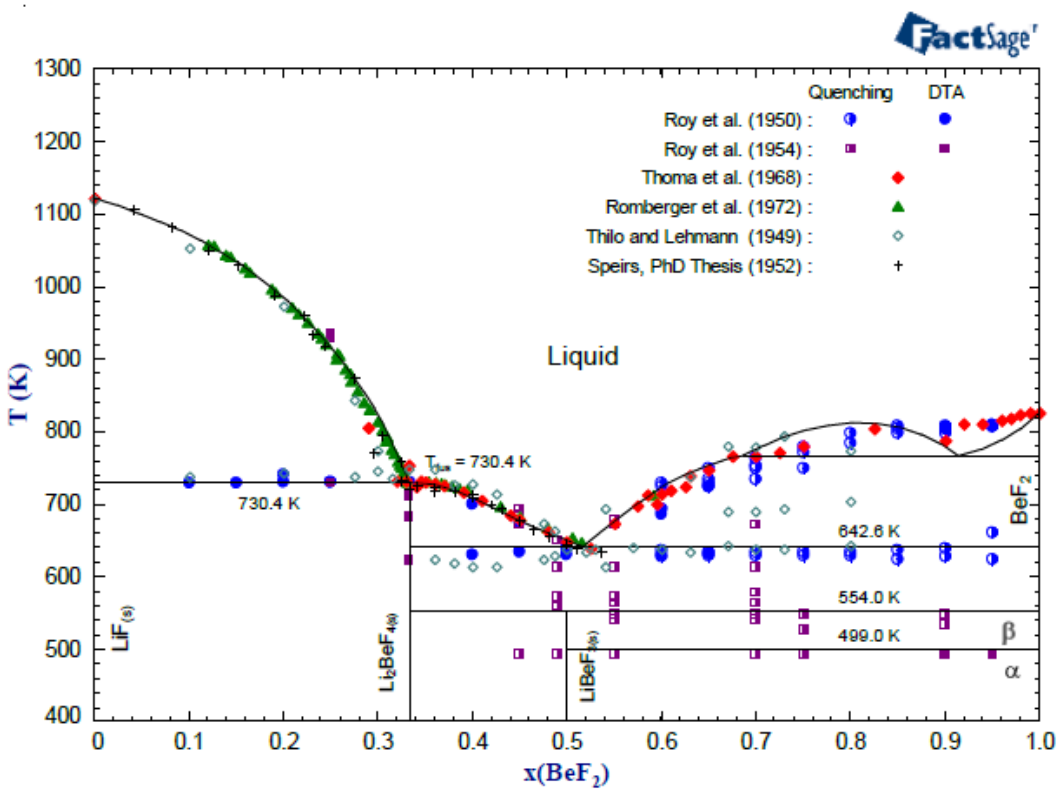

Figure VI-1 : Calculated LiF-BeF_2 phase diagram.

Figure 31. Calculated Multicomponent Phase Diagram with Superimposed Log (p(HF))

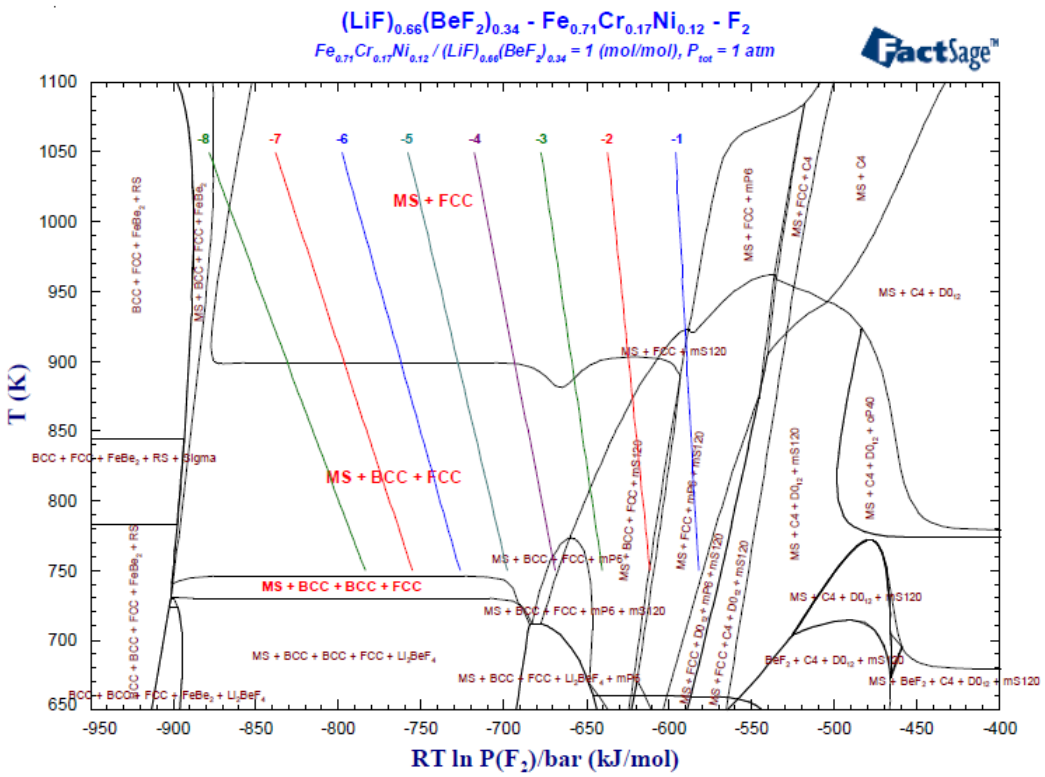

Note: The diagram shows regions of metal stability as well as the concern of $FeBe_2$ formation if conditions are overly reducing.

Figure 32. Schematic of the In-Situ Mechanical (ISM) Testing Systems (left) and an Operational ISM Running a Slow Strain Rate Test in FLiNaK Salt (right)

[[

]]

Figure 33. Comparison of the 316 FLiNaK Fatigue Crack Growth Rate Data with Similar Test Conducted in Air

[[

]]

APPENDIX A. COATINGS, CLADDING, AND TRITIUM MANAGEMENT

The design of the KP-FHR does not require the use of cladding or coatings. However, these materials may be desirable to optimize the performance of the reactor system. [[

]]

Cladding and Coatings

Current ASME Section III Division 5 Code rules for cladded structural components in elevated temperature service are limited. ASME Section III Division 5, Paragraph HBB-2121 allows non-Code qualified materials to be used for cladding if the clad thickness is 10% or less of the thickness of the base material. ASME Section III Division 5, Paragraph HBB-3227.8 specifies that no structural strength will be attributed to the cladding in satisfying the primary load stress limits. It also requires that the cladding will be considered in design evaluation related to limits on deformation-controlled quantities, i.e., strain accumulations due to ratcheting and creep-fatigue damage but does not provide guidance or requirements for that assessment. While the 10% clad thickness rule allows Kairos Power to select corrosion-resistant materials that are not Code qualified for Class A service, the lack of design rules presents challenges in their application.

In order to help enable the application of corrosion-resistant coatings and cladding, Kairos Power has completed a GAIN research collaboration (References 70, 71, 72, and 73) (Gain cladding project under contract No. DE-AC02-06CH11357 with the US Department of Energy). The GAIN research includes establishing the mechanical nature of the cladding or coating (compliant or elastic), determining key mechanical properties (yield strength, creep rate), assessing the integrity of the coating after thermal cycling, and testing the environmental compatibility of the cladding or coating in molten Flibe salt. This program is expected to result in the ability to use cladding and coatings with ASME Section III Division 5 structural materials.

Coatings and claddings used in the KP-FHR to decrease tritium permeability will potentially be applied to salt facing surfaces because the benefit of a tritium permeation barrier is expected to increase for salt facing applications compared to the air side. Since the tritium permeation barrier coatings and claddings will be exposed to molten Flibe, the corrosion resistance of barrier materials will be evaluated, and the selection of tritium permeation barrier materials will be limited to those which provide comparable or improved corrosion rates in Flibe compared to Alloy 316H. In addition to Flibe facing tritium permeation barriers, the KP-FHR design may also include nitrate salt-facing coatings which would assist in reducing the permeation of tritium through the intermediate loop piping.

[[

]]

[[
]]

Cladding and Coatings for Air Side Applications

For the application of cladding or coatings on the air side of safety-related systems, there are no ASME design rules governing their use. Potential applications for coatings on the air side of these systems include oxide films [[ ]] surface treatments to enhance thermal emissivity or providing anti-galling. If coatings are used on the air side of safety-related systems, the benefit of the treatment will be demonstrated and confirmed through analysis and/or testing that there is no significant degradation to the underlying structural material.

APPENDIX B. INSPECTION AND AGING MANAGEMENT

Introduction

Nuclear Power Plant component life management requires a combination of analysis, inspection, testing, and monitoring activities. The information derived from each of these activities complements one another and should be utilized as part of an integrated program. Qualification through mechanical and environmental testing is the first step in ensuring material performance for long-term service in nuclear power plants. While test plans can to some extent account for combinations of mechanical and environmental factors that affect material performance, it is rare that laboratory testing can account for all of the variables and interactions present during reactor operation. Furthermore, it is often impractical to perform laboratory tests for times on the order of the expected component lifetimes (usually decades). While the material qualification test programs described in this document provide confidence that Alloy 316H / ER16-8-2 will perform satisfactorily over the service life of the plant; in-service monitoring and evaluation throughout the plant life will be used to further ensure the safe and reliable operation of the KP-FHR.

Inspection and Monitoring Program

ASME Section XI has historically provided rules for in-service inspection and the replacement and repair of components during the operating life of light water reactors. The unique physical features of high temperature reactors such as the KP-FHR present a new paradigm for the Reliability and Integrity Management (RIM) that has required the Code to develop new approaches. The new approach being implemented as ASME Section XI Division 2 “Reliability”, applies to any type of reactor design and was published for the first time in the 2019 Edition of the ASME code.

For both the non-power test reactor and commercial power reactor systems a materials surveillance system will be used to assess the combined effects of molten salt and irradiation on structural materials. The location of the materials surveillance system for the non-power test reactor is planned to be outside of the core and within the graphite reflector. At the location of the metallic samples, the samples should see a flux of 0.02-0.03 dpa/year so that in a relatively short exposure time (~1 year exposure) a significant degree of irradiation could be produced and assessed via subsequent post-irradiation examination. The bounding dpa for the reactor vessel is <0.1 dpa at the end of life, so that 0.02 dpa represents a meaningful degree of damage.

In the materials surveillance system program, representative weld metal, base metal, and heat affected zone samples will assessed for the potential occurrence of irradiation affected corrosion and stress corrosion cracking. For Irradiation-Assisted Stress Corrosion Cracking, fracture mechanics samples will be used that approximate the conditions of the in-Flibe testing, i.e., K_I~25 MPa$\sqrt{m}$ at an average temperature between 550-650°C. One difference is that these samples will be loaded via constant displacement rather than tested at constant K_I. The details of the surveillance coupon program (sample types, numbers, etc.) will be provided at the time of the operating license application.

For both the non-power test reactor and the commercial power reactor systems, inspection and monitoring programs to further ensure material and component performance will be utilized. These efforts will involve on-line monitoring systems as well as periodic inspections. A number of technologies

are currently being assessed and developed to facilitate these programs that are applicable to the non-destructive inspection of the reactor vessel. For the non-power test reactor, the details of the inspection and monitoring programs will be provided at the time of the operating license application.

For the commercial power reactor, inspection and monitoring will be performed in accordance with the requirements of ASME Section XI 2019 Edition, Mandatory Appendix I ("RIM Decision flowcharts for use with the RIM") and Appendix II ("Derivation of component reliability targets from plant safety requirements"). Component Level Reliability Requirements will be derived from Plant Level Reliability Requirements through the Probabilistic Risk Assessment process. With Reliability Targets established, components will be assessed for mechanisms of environmental degradation and modes of failure as derived from the Phenomenon Identification and Ranking Table. Critical flaw size will be determined for the most likely modes of failure in each component. Monitoring and Non-Destructive Examination technologies will be evaluated for the capability to detect sub-critical flaws and to endure the relevant inspection environments. Technologies and inspection schedules will then be selected for each area of interest to ensure that flaws can be detected before they grow to critical flaw size. Material performance will be monitored during operation, and data will be fed back to update the Monitoring and Non-Destructive Examination (MANDE) schedule throughout the life of the plant. The specific details of a RIM program for the commercial power reactor will be provided with the operating license application.

The new RIM allows a combination of MANDE methods for an aging management program. The ability to use both monitoring and non-destructive examination is a significant advantage to many advanced reactor designs, including the KP-FHR, since their compact size and need for coolant chemistry control limits access to some components during the operating lifetime of the plant. While the 2019 Edition of ASME Section XI Division 2 outlines the top-level requirements for a RIM program, Mandatory Appendix VII of Division 2 will describe the specific MANDE methods and acceptance criteria for each of the different types of advanced reactors. Note that Article VII-4 has been reserved for Molten Salt Reactors (and presumably FHR designs) but has not yet been developed in detail. Kairos Power is active with the Section XI Committee Sub-Groups and Working-Groups related to RIM and MANDE and plans to apply the KP-FHR experience to the development of relevant Code articles for FHRs.

APPENDIX C. DETAILS OF THE CORROSION DATA ANALYSIS

Many testing programs that are expected to yield quantitative results were developed with the intent of statistical analysis of the data. For example, the general corrosion testing of Alloy 316H and ER16-8-2 plans include three samples per condition, conducted over a wide range of times and temperatures. These data will be analyzed via electron microscopy of corrosion coupon cross sections which, we believe, is superior and more sensitive a measure than weight change.

With those corrosion data, Kairos Power will develop 'baseline' corrosion models for Alloy 316H and ER16-8-2 and conduct separate effects tests to assess key variables that include microstructure, contaminants, redox control, occluded geometry, and erosion-corrosion. Statistical analysis such as Analysis of Variance (ANOVA) will be used to establish the significance of these variables on the response model of corrosion rate compared to random error. Furthermore, the corrosion model will utilize appropriate prediction bands to ensure appropriate and conservative extrapolation from test conditions to KP-FHR operational times and temperatures.

Note that some testing may not be amenable to statistical analysis but is being performed to develop understanding and guidance. For example, the slow strain rate tests in Flibe are being performed primarily to assess regimes in which environmentally assisted cracking may occur. In these tests, a change in response (load vs. stroke) relative to air testing and post-test analysis of the fracture path will be used to develop understanding of the degree of concern for cracking. Similarly, stress corrosion cracking tests are being conducted to better understand if this phenomenon occurs in environments and mechanical conditions of relevance to the KP-FHR. Depending on the response of Alloy 316H and ER16-8-2 to these tests, a statistical analysis of the data may be used but also may employ fundamental materials science and engineering judgement to develop appropriate design factors or other practices (e.g., periodic inspection) that will appropriately address the concern of environmentally assisted cracking.

Note that corrosion rates can be confounded by complicating factors such as carbon pickup during testing as well as the difficulty in removing dried salt from test coupons. To mitigate these factors, Kairos Power will use electron microscopy of corrosion coupon cross sections as the primary method to assess corrosion (e.g., depth of chromium loss) as well as other compositional changes (e.g., the extent of Fe and Ni loss, the precipitation of Mo-rich Laves phase, and the precipitation of carbon rich phases). An example of this analysis is given below in Appendix C, Figure 1.

For information, an example of expected statistical analysis of corrosion data is presented below. In this example, the corrosion data of Zheng et al. (pink squares) are used to generate example corrosion data for three different temperatures and for times up to 10,000 hours (Reference 18). The example data are shown below in Appendix C, Figure 2.

An example of how these data may be fit is via Appendix C, Equation C-1. In Equation C-1, A is a fitting constant, t is the exposure time, n is a fitting constant (equal to 0.5 for mass diffusion control), Q is the apparent activation energy, R is the gas constant and T the temperature.

$$Cr\ loss\ depth = A * t^n * EXP(-Q/RT) \qquad \text{Eq. C-1}$$

The fit of the data to the combined model is shown by the blue surface in Appendix C, Figure 3. In this manner all the data (example data in gray circles, Zheng data in pink squares) can be used to increase the confidence in extrapolating to the conditions of the KP-FHR. For example, the reactor vessel will operate at approximately 550°C for [[ ]] which would exhibit <10 microns of corrosion (Cr loss) via the best estimate prediction of this model. The example baseline model is shown in two dimensions in Appendix C, Figure 4 (upper graph) with 95% prediction intervals. In Appendix C, Figure 4, an example of a separate effects corrosion test is shown (lower plot) along with how a factor of improvement may be defined. In this example, the factor of improvement is conservatively determined at an exposure time within the data and between the baseline model lower bound and the separate effects test upper bound.

Appendix C Figure 1. Example of How a Corrosion Coupon was Sectioned (left) and Corresponding Compositional Maps for Iron, Chromium, and Nickel

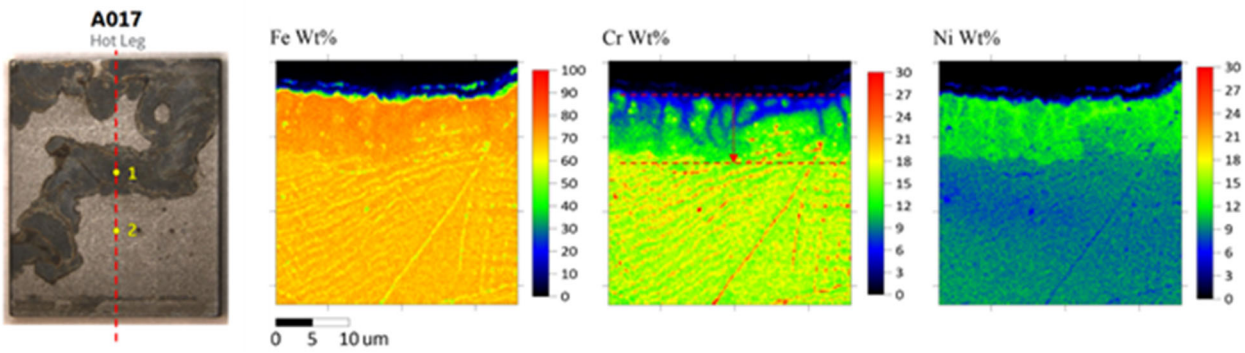

Appendix C Figure 2. The Corrosion Data of Alloy 316L in Flibe of Zheng (Pink Squares) Compared to Example Data at Three Different Temperatures

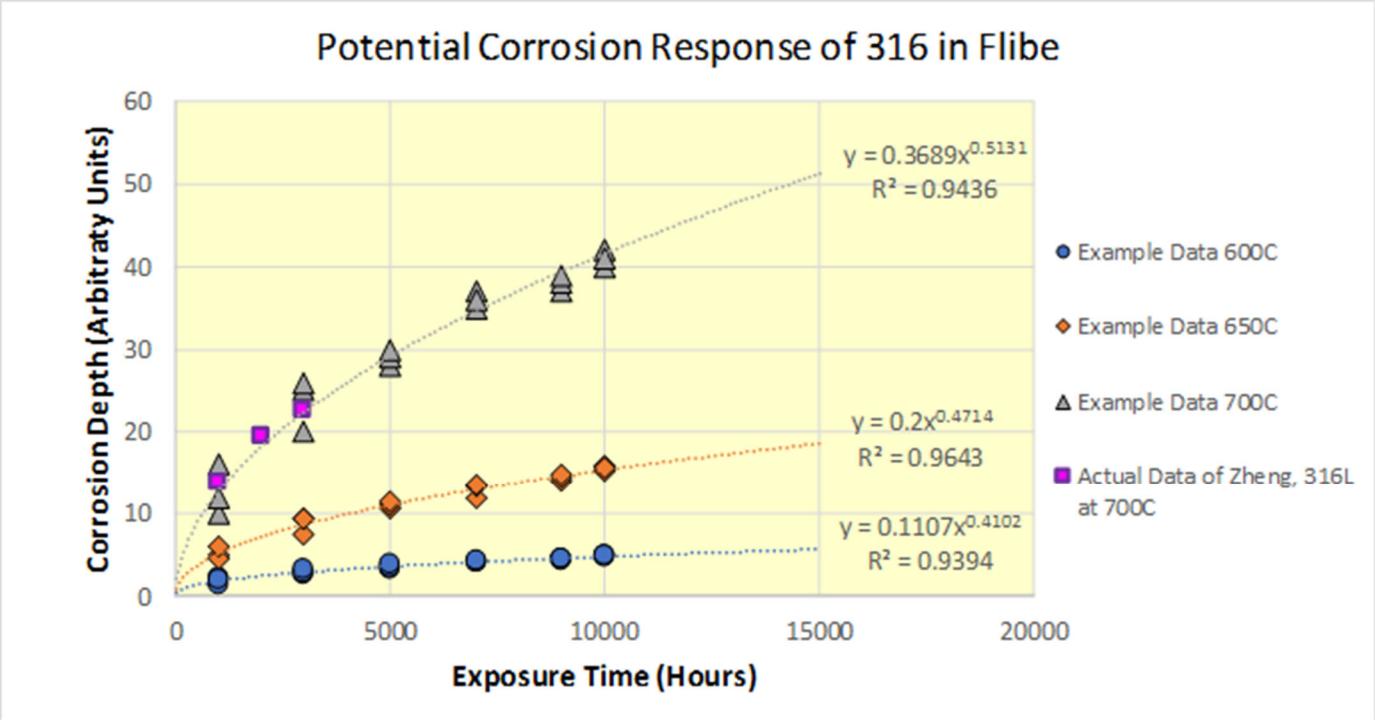

Appendix C Figure 3. Example of How Corrosion Data May be Fit and Extrapolated to Times Out to 20 years

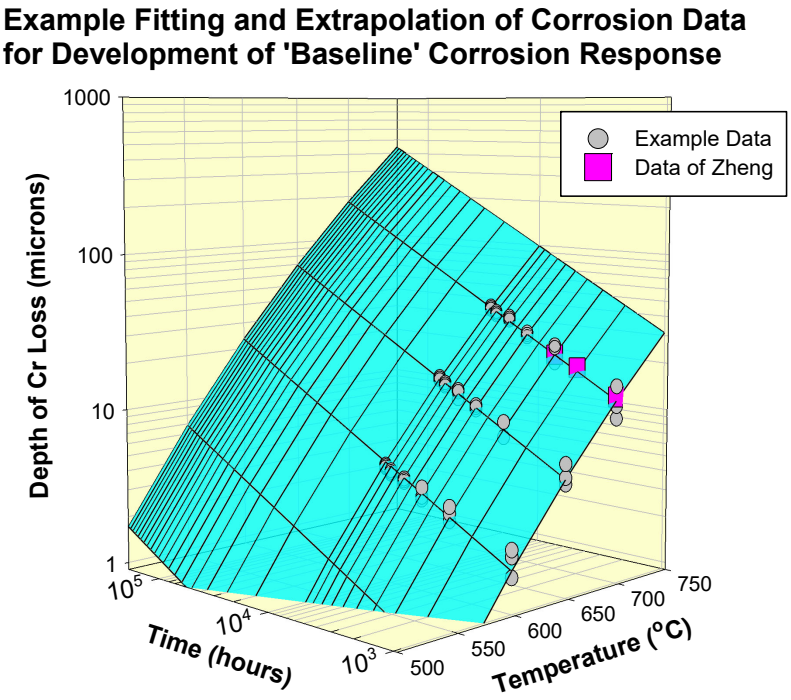

Appendix C Figure 4. Example of How the Baseline Corrosion Model May be Compared to a Separate Effects Test to Determine a Factor of Improvement

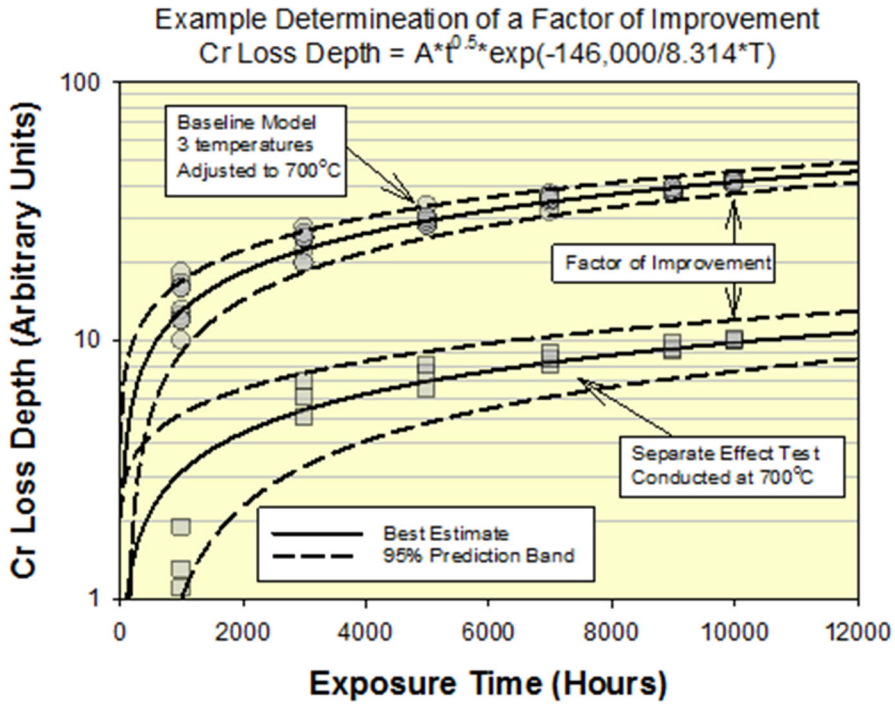

APPENDIX D. NOT USED

APPENDIX E. NOT USED

APPENDIX F. CERTIFIED MATERIAL REPORTS

Appendix F Figure 1. Material Certification Report for Alloy 316H Plate

[[

]]

Appendix F Figure 2. Overcheck of the Composition of the Alloy 316H Plate

[[

]]

Appendix F Figure 3. Material Certification Report for the ER16-8-2 Weld Wire

[[

]]

Appendix F Figure 4. Material Certification Report for Second Heat of ER16-8-2

[[

]]

Appendix F Figure 5. Material Certification Report (tentative) for a Third Heat of ER16-8-2

[[

]]